HCV infection activates the proteasome via PA28γ acetylation and heptamerization to facilitate the degradation of RNF2, a catalytic component of polycomb repressive complex 1.

Hirotake Kasai[1], Atsuya Yamashita[1], Yasunori Akaike[1], Tomohisa Tanaka[1, 4], Yoshiharu Matsuura[2, 3], and Kohji Moriishi[1, 4].

[1] Department of Microbiology, Faculty of Medicine, Graduate Faculty of Interdisciplinary Research, University of Yamanashi, Yamanashi 409-3898, Japan.
[2] Laboratory of Virus Control, Research Institute for Microbial Diseases (RIMD), Osaka University, Osaka 565-0871, Japan.
[3] Center for Infectious Diseases Education and Research (CiDER), Osaka University, Osaka 565-0871, Japan.
[4] Division of Hepatitis Virology, Institute for Genetic Medicine, Hokkaido University, Hokkaido 060-0808, Japan

Running title: The mechanism by which HCV infection impairs polycomb repressive complex 1 activity.

Corresponding author: Kohji Moriishi, D.V.M., Ph.D.
Department of Microbiology, Faculty of Medicine, Graduate Faculty of Interdisciplinary Research, University of Yamanashi, Yamanashi 409-3898, Japan
Tel: +81-55-273-9537; Fax: +81-55-273-6728
Email: kmoriishi@yamanashi.ac.jp

ABSTRACT

We previously reported that hepatitis C virus (HCV) infection or HCV core protein expression induces HOX gene expression by impairing histone H2A monoubiquitination via a proteasome-dependent reduction in the level of RNF2, a key catalytic component of polycomb repressive complex 1 (PRC1) (J. Virol, 2021, 95, e01784-20). In this study, we aimed to investigate the mechanism by which HCV infection accelerates RNF2 degradation. Yeast two-hybrid screening and an immunoprecipitation assay revealed that RNF2 is a PA28γ-binding protein. The proteasome activator PA28γ destabilized the RNF2 protein in a proteasome-dependent manner, since RNF2 degradation was impaired by PA28γ knockout or MG132 treatment. HCV infection or core protein expression reduced the levels of RNF2 and histone H2A K119 monoubiquitination and induced the expression of HOX genes in the presence of PA28γ, while PA28γ knockout reversed these changes. Treatment with a lysine acetyltransferase inhibitor inhibited the acetylation of PA28γ at K195 and the degradation of the RNF2 protein, while treatment with a lysine deacetylase inhibitor accelerated these events in a PA28γ-dependent manner. RNF2 protein degradation was increased by expression of the acetylation mimetic PA28γ mutant but not by expression of the acetylation-defective mutant or the proteasome activation-defective mutant. Furthermore, HCV infection or core protein expression facilitated the interaction between PA28γ and the lysine acetyltransferase CBP/p300 and then accelerated PA28γ acetylation and heptamerization to promote RNF2 degradation. These data suggest that HCV infection accelerates the acetylation-dependent heptamerization of PA28γ to increase the proteasomal targeting of RNF2.

IMPORTANCE: HCV is a causative agent of HCV-related liver diseases, including hepatic steatosis, cirrhosis and hepatocellular carcinoma. PA28γ, which, in heptameric form, activates the 20S core proteasome for the degradation of PA28γ-binding proteins, is responsible for HCV-related liver diseases. HCV core protein expression or HCV infection accelerates RNF2 degradation, leading to the induction of HOX gene expression via a decrease in the level of H2Aub on HOX gene promoters. However, the mechanism of RNF2 degradation in HCV-infected cells has not been clarified. The data presented in this study suggest that PA28γ acetylation and heptamerization are promoted by HCV infection or by core protein expression to activate the proteasome for the degradation of RNF2 and are responsible for HCV propagation. This study provides

novel insights valuable for the development of therapies targeting both HCV propagation and HCV-related diseases.

KEYWORDS: HCV, RNF2, H2A monoubiquitination, PA28γ/REGγ/PMSE3/Ki

INTRODUCTION

Hepatitis C virus (HCV) is a major human pathogen that is currently causing chronic infection in 50 million people worldwide, with approximately 1.0 million new infections occurring annually, and puts infected individuals at risk of hepatic steatosis, liver cirrhosis, and hepatocellular carcinoma (HCC) (1). The development of direct-acting antiviral agents (DAAs) against HCV has led to significant improvements in the treatment of HCV infections over the past decade (2, 3). However, it has also been reported that hepatitis C patients remain at risk of HCC even after viral elimination (2). Understanding the pathogenesis of HCV infection remains an important challenge for the development of effective hepatitis C therapies. HCV belongs to the genus *Hepacivirus* in the *Flaviviridae* family and possesses an enveloped nucleocapsid containing a positive-sense RNA genome with a length of 9.6 kb. The single polyprotein (~ 3000 amino acids) encoded by the viral genome is cleaved by viral and host proteases into 10 final viral proteins, which are classified as structural or nonstructural proteins (4). The structural proteins are the core, E1 and E2 proteins, and the nonstructural proteins are the p7, NS2, NS3, NS4A, NS4B, NS5A, and NS5B proteins. Nonstructural proteins play important roles in viral genome replication, assembly, and budding, whereas structural proteins, together with the host lipid bilayer, form viral particles (4). The core protein, a component of the nucleocapsid, has been implicated in the formation of viral particles as well as the induction of HCV-related pathological changes (4). Mice expressing the core protein in the liver were found to exhibit HCV-related liver diseases such as type II diabetes mellitus (5), hepatic steatosis (6, 7), and HCC (8, 9), suggesting that the core protein plays an important role in inducing HCV-related pathological changes.

We previously reported that the HCV core protein can promote a reduction in the monoubiquitination of lysine (K) 119 of histone H2A in the promoter regions of HOX alleles and subsequently activate the transcription of HOX genes (10). HOX family genes, a set of 39 genes divided into 4 clusters, namely, HOXA, HOXB, HOXC and

93 HOXD, regulate body plan development during the neonatal stage and also regulate the
94 growth, survival, migration and invasion of cells to support cancer development (11,
95 12). Monoubiquitination of H2A at K119 is catalysed by polycomb repressive complex
96 1 (PRC1) to repress target genes (13). The expression of the HCV core protein was
97 found to increase the degradation of the RNF2 protein, a main catalytic component of
98 PRC1, and reduce the level of K119-monoubiquitinated histone H2A (H2Aub) on the
99 promoter regions of HOX alleles (10). The core protein-dependent degradation of RNF2
100 was found to be independent of polyubiquitination and to be inhibited by treatment with
101 the proteasome inhibitor MG132 (10). However, the molecular mechanism by which the
102 core protein induces polyubiquitination-independent, proteasome-dependent
103 degradation of RNF2 remains unclear.
104 The ubiquitin–proteasome system is a major proteolytic pathway that regulates
105 various intracellular functions. The proteasome complex consists of the 20S proteolytic
106 core and several proteasome activators (PAs), including the 19S PA (PA700), 11S PA
107 (PA28 or REG), and PA200. The 19S PA can bind to the 20S proteasome and activate
108 polyubiquitination-dependent proteolysis (14), while the 11S PA can bind to the 20S
109 proteasome and activate polyubiquitin-independent proteolysis (14). The 11S PA is
110 classified as a PA28α/PA28β heteroheptamer or a PA28γ homoheptamer. The
111 expression of PA28α and PA28β is induced by interferon (IFN)-γ for the processing of
112 MHC class I peptides (14). The PA28α/PA28β heteroheptamer activates the
113 chymotrypsin-like activity of the 20S core proteasome (CP) in the cytoplasm, while the
114 PA28γ homoheptamer activates the trypsin-like activity of the 20S CP in the nucleus
115 (15). Several proteins, such as AID, SRC-3, p19, the HCV core protein and SirT1, have
116 been reported to be substrates of the PA28γ-dependent proteasome system (4, 16-18).
117 The amino acid sequence of human PA28γ is identical to that of its murine homologue
118 and shares 55% identity with that of its tick homologue (19), suggesting that PA28γ is
119 highly conserved from insects to mammals. This broad conservation indicates that
120 PA28γ may regulate fundamental functions across the animal kingdom, although its
121 detailed biological function is largely unknown. We previously reported that PA28γ
122 binds to the HCV core protein and promotes the degradation of unfolded or
123 nonfunctional core proteins through a polyubiquitin-independent proteosomal pathway
124 (20, 21). Furthermore, PA28γ knockout abolished core protein-related liver defects
125 (type II diabetes, steatosis, and HCC) in mice, suggesting that PA28γ plays a critical

126 role in core protein-induced pathological changes (22, 23). Phenotypic analysis of
127 PA28γ-knockout mice revealed that they were viable and capable of mating but
128 exhibited mild growth defects (24), decreased sperm fertility (25), and accelerated
129 senescence (26), although a critical function of PA28γ has not yet been identified.
130 In this study, we identified RNF2 as a novel PA28γ-binding protein and
131 examined the effect of PA28γ on the stability of RNF2, monoubiquitination of histone
132 H2A, regulation of HOX gene transcription, and propagation of HCV. We also aimed to
133 clarify the mechanism by which the HCV core protein regulates PA28γ-dependent
134 proteasome activity to inhibit PRC1 activity in HCV-infected cells.
135
136 **RESULTS**
137 **PA28γ interacted with RNF1 and RNF2, components of polycomb repressor**
138 **complex 1.**
139 To identify novel PA28γ-binding molecules, we screened a human foetal brain library
140 using a yeast two-hybrid system with PA28γ as bait. We identified four positive clones,
141 Cl-26, Cl-49, Cl-50 and Cl-53. Cl-26 included the gene encoding RNF1 in the open
142 reading frame of GAL4-DNA binding domain, while Cl-49 included the gene encoding
143 PA28γ in the frame. Cl-50 and Cl-53 included partial regions of the gene encoding
144 pyruvate dehydrogenase complex component X isoform, but they did not match the
145 frame. RNF1, a component of PRC1, was identified as a PA28γ-binding partner by this
146 yeast two-hybrid screen. Since RNF2 is a catalytic component of PRC1 and is a
147 homologue of RNF1, the RNF2 gene was isolated from total cDNA of the human liver.
148 Plasmids encoding N-terminal FLAG-tagged PA28γ (FLAG-PA28γ), N-terminal HA-
149 tagged RNF1 (HA-RNF1) and N-terminal HA-tagged RNF2 (HA-RNF2) were
150 constructed to examine the interactions of PA28γ with RNF1 and RNF2 by
151 immunoprecipitation in 293T cells. HA-RNF1 or HA-RNF2 was coimmunoprecipitated
152 with FLAG-PA28γ, while FLAG-PA28γ was reciprocally coimmunoprecipitated with
153 HA-RNF1 or HA-RNF2 (Fig. 1A). Next, we examined the subcellular localization of
154 PA28γ and RNF2 by immunofluorescence staining. Unfortunately, we could not find an
155 antibody that reacts specifically with endogenous RNF1. However, PA28γ and RNF2
156 were partially colocalized in the nucleus (Fig. 1B). The fluorescence intensities of
157 PA28γ (green) and RNF2 (red) within each pixel were quantified and plotted (Fig. 1C),
158 revealing a significant negative correlation for the colocalization of these two proteins

159 (R = -0.856, Fig. 1C). These data suggest that PA28γ binds to RNF2 but is not strongly
160 colocalized with RNF2 in untreated cells.
161
162 **PA28γ reduced the stability of RNF1 and RNF2**
163 We hypothesized that the intracellular segregation of PA28γ and RNF2 may be
164 due to PA28γ-dependent degradation of RNF2 following the interaction between these
165 two proteins, because PA28γ-binding proteins are reportedly degraded via a
166 polyubiquitin-independent proteosomal pathway (15). Using the CRISPR-Cas9 system,
167 we established a PA28γ-knockout cell line and then examined the stability of the RNF1
168 and RNF2 proteins via a cycloheximide (CHX) chase assay. PA28γ was detected in
169 wild-type Huh7OK1 cells, which are highly permissive to HCV infection (27), but not
170 in PA28γ-knockout Huh7OK1 cells (Fig. 2A, B). The level of RNF2 in the wild-type
171 cells was reduced by less than 50% 2 h after CHX treatment, whereas no significant
172 reduction in the RNF2 level was observed in the PA28γ-knockout cells (Fig. 2A, B).
173 RNF1 tended to be less stable in PA28γ-knockout cells than in wild-type cells, but the
174 difference was not significant (Fig. 2A, B). In addition, the stability of BMI1 (PCGF4),
175 another component of PRC1, was not affected by PA28γ knockout (Fig. 2A, B). These
176 data suggest that PA28γ destabilizes RNF2.
177 When PA28γ expression was restored in PA28γ-knockout cells, the
178 endogenous RNF1 and RNF2 protein levels decreased in a PA28γ dose-dependent
179 manner (Fig. 3A). However, the RNF1 and RNF2 mRNA levels were not affected by
180 restoration of PA28γ expression (Fig. 3B). Furthermore, restoring the expression of
181 PA28γ reduced the levels of HA-RNF1 and HA-RNF2 (Fig. 3C). HA-RNF1 and HA-
182 RNF2 was expressed separately in 293T cells and were then isolated by
183 immunoprecipitation using an anti-HA antibody for *in vitro* proteasome assays. The
184 immunoprecipitates containing HA-RNF1 or HA-RNF2 were mixed with recombinant
185 20S CP with or without the 11S PA consisting of PA28γ. The levels of HA-RNF1 and
186 HA-RNF2 were reduced in the presence but not in the absence of the 11S PA. These
187 results suggest that PA28γ is involved in the proteolysis of RNF1 and RNF2. Since the
188 RNF2 protein was more strongly destabilized by PA28γ than was the RNF1 protein, we
189 subsequently focused on the relationship between RNF2 and PA28γ.
190
191 **PA28γ promoted proteasome-dependent degradation of the RNF2 protein.**

192 PA28γ increases the trypsin-like activity of the ubiquitin-independent proteasome
193 (15). We next examined the effect of proteasome activity on RNF2 stability in the
194 presence of PA28γ. The RNF2 protein level was reduced in PA28γ-knockout cells by
195 restoration of PA28γ expression, while MG132 treatment suppressed the PA28γ-
196 dependent decrease in the RNF2 protein level (Fig. 4A). The intracellular localization of
197 PA28γ and RNF2 was evaluated in the presence and absence of MG132. RNF2 was
198 partially colocalized with PA28γ in the absence of MG132, while it strongly colocalized
199 with PA28γ in the presence of MG132 (Fig. 4B). A significant negative correlation for
200 the colocalization of wild-type PA28γ and RNF2 was found in the cells (Fig. 4C, a left
201 half). The PA28γ mutant in which proline 245 (Pro245) was replaced with tyrosine
202 (Tyr; PA28γP245Y) could not activate the proteasome (21, 28). This mutation lost the
203 negative correlation between PA28γ and RNF2 localizations (Fig. 4C, a right half).
204 These data suggest that PA28γ promotes the proteolytic degradation of RNF2 in a
205 proteasome-dependent manner.
206
207 **PA28γ impaired the monoubiquitination of histone H2A at K119 and induced the**
208 **transcription of HOX genes.**
209 PRC1 monoubiquitinates K119 of histone H2A to suppress the transcription of target
210 genes via chromatin compaction (13, 29). RNF2 is an E3 ubiquitin ligase responsible
211 for the catalytic activity of PRC1 for the monoubiquitination of histone H2A at K119
212 (13, 30, 31). We next examined the effects of PA28γ expression on histone H2A
213 monoubiquitination and on the transcription of HOX genes. Restoration of PA28γ
214 expression reduced the level of H2Aub (Fig. 5A) in PA28γ-knockout cells but did not
215 affect the level of total histone H2A. We previously reported that HOXB9, HOXC13,
216 and HOXD13 were completely silenced in Huh7OK1 cells but HOXA1 and HOXA3
217 was not (10). We evaluated the effect of PA28γ expression on the expression of the
218 group with HOX gene silencing. Restoring the expression of PA28γ in PA28γ-knockout
219 cells induced the transcriptional activation of HOXB9 (Fig. 5B). The level of H2Aub in
220 the promoter region of HOXB9 was then evaluated by a chromatin immunoprecipitation
221 (ChIP) assay and was found to be reduced by the restoration of PA28γ expression in
222 PA28γ-knockout cells (Fig. 5C). The HOXB1, HOXC13 and HOXD13 genes were also
223 transcriptionally activated by PA28γ expression (Fig. 5D), whereas HOXA1 and
224 HOXA3 gene transcription was not affected by the restoration of PA28γ expression in

225 PA28γ-knockout cells (Fig. 5D). These data suggest that PA28γ reactivates the
226 expression of silenced HOX genes via impairment of H2A monoubiquitination.
227
228 **HCV infection impaired the monoubiquitination of histone H2A at K119 and**
229 **reduced the level of RNF2 in a PA28γ-dependent manner.**
230 We previously showed that HCV infection promoted RNF2 protein degradation via a
231 polyubiquitination-independent proteasome pathway and subsequently reduced the level
232 of H2Aub in the promoter regions of HOX genes (10). When wild-type Huh7OK1 cells
233 were infected with HCV, the levels of H2Aub and RNF2 were reduced in a manner
234 dependent on the number of days after infection in the presence but not in the absence
235 of PA28γ (Fig. 6A, B). Knocking out PA28γ did not affect HCV replication, although it
236 increased the level of the HCV core protein in cells and reduced the levels of both HCV
237 RNA and infectious viral particles in the culture supernatant (Fig. 6C), consistent with
238 the data shown in our previous report (21). These findings suggest that HCV infection
239 impairs the monoubiquitination of histone H2A and the stability of RNF2 in a PA28γ-
240 dependent manner.
241
242 **The HCV core protein reduced the level of H2Aub in the promoter regions of**
243 **HOX genes and promoted their transcription in the presence but not in the**
244 **absence of PA28γ.**
245 Our previous report suggested that polyubiquitination-independent proteolysis of
246 RNF2 is promoted by the expression of the HCV core protein to activate HOX gene
247 transcription in HCV-infected cells (10). Next, we examined whether the expression of
248 the HCV core protein affects the RNF2 protein level, the H2A monoubiquitination level
249 and HOX gene transcription in the presence or absence of PA28γ. Expression of the
250 core protein reduced the levels of H2Aub and RNF2 in the presence but not in the
251 absence of PA28γ, although the level of the core protein was markedly higher in
252 PA28γ-knockout cells than in wild-type cells (Fig. 7A). A ChIP assay was carried out to
253 estimate the level of H2Aub in the HOXB9 promoter region. The level of H2Aub in the
254 HOXB9 promoter region was reduced by expression of the core protein in the presence
255 but not in the absence of PA28γ (Fig. 7B). On the other hand, core protein expression
256 promoted the transcription of the HOXB9 gene in the presence but not in the absence of
257 PA28γ (Fig. 7C). These data suggest that the core protein reduces the levels of RNF2

258 and H2Aub and increases the expression of HOX gene in the presence but not in the
259 absence of PA28γ.
260
261 **Acetylation of PA28γ at Lys195 promoted its homoheptamerization and RNF2**
262 **degradation.**
263 PA28γ was reported to be acetylated at Lys195 (K195) to promote its
264 homoheptamerization for 20S CP binding and proteasome activation (32). CBP/p300, a
265 lysine acetyltransferase (KAT), was reported to be responsible for the acetylation of
266 PA28γ at K195 (32). Moreover, the core protein can interact with CBP and increase its
267 acetyltransferase activity (33). We hypothesized that the core protein promotes CBP-
268 dependent acetylation of PA28γ and augments the homoheptamerization of PA28γ to
269 activate the proteasome to target RNF2 for degradation. We examined the effect of the
270 KAT inhibitor C646 on PA28γ-dependent RNF2 degradation. Restoring the expression
271 of PA28γ reduced the RNF2 level in PA28γ-knockout cells; in addition, CHX treatment
272 promoted the reduction in the RNF2 level in the presence of PA28γ, whereas C646
273 treatment impaired the reduction in the RNF2 level in the presence of PA28γ regardless
274 of CHX treatment (Fig. 8A). Immunoprecipitation using an anti-acetylated lysine (Ace-
275 K) antibody and the lysates used to acquire the data shown in Fig. 8A showed that C646
276 treatment suppressed PA28γ acetylation (Fig. 8B). On the other hand, treatment with the
277 lysine deacetylase inhibitor trichostatin A (TSA) promoted the decrease in the RNF2
278 level in the presence but not in the absence of PA28γ (Fig. 8C), while TSA treatment
279 increased PA28γ acetylation (Fig. 8D). PA28γK195R, in which Lys195 is replaced with
280 Arg, is an acetylation-defective mutant, while PA28γK195Q, in which Lys195 is
281 replaced with Gln, is an acetylation mimetic mutant (32). A CHX chase assay was
282 carried out to investigate the stability of RNF2 in the presence of wild-type PA28γ or
283 these mutants. Six hours after treatment with CHX, the RNF2 level was 21% of that in
284 the control cells in the cells expressing wild-type PA28γ, 104% of that in the control
285 cells in the cells expressing PA28γK195R and 14% of that in the control cells in the
286 cells expressing PA28γK195Q. These results suggest that the regulation of PA28γ
287 acetylation controls the PA28γ-dependent degradation of RNF2. The HCV core protein
288 increased the degradation of RNF2 in the absence but not in the presence of C646,
289 suggesting that the core protein promotes the PA28γ-dependent degradation of RNF2

290 via KAT activation. These data suggest that HCV infection or the core protein
291 expression promotes PA28γ acetylation for destabilization of RNF2.
292
293 **HCV infection promoted the acetylation of PA28γ via CBP activity.**
294 We investigated the mechanism by which HCV infection or core protein expression
295 promotes PA28γ acetylation. Huh7OK1 cells were infected with HCV, and the infected
296 cells were harvested at 0, 3 and 6 dpi. The cell lysates were subjected to
297 immunoprecipitation using rabbit anti-Ace-K IgG or normal rabbit IgG. The levels of
298 acetylated PA28γ and PA28γ homoheptamers increased in a time-dependent manner
299 after infection (Fig. 9A, B). When PA28γ expression was restored with or without the
300 expression of the core protein in PA28γ-knockout cells, the core protein promoted
301 PA28γ acetylation and homoheptamerization (Fig. 9B, C), consistent with the data
302 shown in Fig. 9A. The core protein has been reported to interact with CBP and
303 subsequently increase its acetyltransferase activity (33). EGFP-PA28γ and FLAG-CBP
304 were coexpressed in PA28γ-knockout cells, and EGFP-PA28γ coimmunoprecipitated
305 with FLAG-CBP (lane 4, Fig. 9D). Furthermore, the core protein increased the amount
306 of EGFP-PA28γ coimmunoprecipitated with CBP (lane 5, Fig. 9D). The RNF2 protein
307 level was decreased in HCV-infected cells but was restored by CBP knockdown in
308 infected cells (Fig. 9E). Taken together, these results suggest that the HCV core protein
309 in infected cells reinforces the interaction between PA28γ and CBP, induces the
310 acetylation and homoheptamerization of PA28γ, and activates the proteasome for RNF2
311 degradation.
312
313 **DISCUSSION**
314 Alterations in gene expression patterns in HCV-infected cells or liver tissue
315 of individuals with hepatitis C may be involved in the pathogenic mechanism of HCV
316 (34). We previously reported that HCV infection impaired PRC1-dependent
317 monoubiquitination of histone H2A at K119 on HOX alleles through degradation of
318 RNF2, which subsequently induced the expression of HOX genes (10). The data in this
319 previous report also suggested that RNF2, a catalytic component of PRC1, is degraded
320 in response to HCV infection or core protein expression and that this degradation is
321 dependent on the proteasome but not on polyubiquitination (10). However, the
322 mechanism by which the core protein induces the degradation of RNF2 after infection

323 has not been elucidated. Furthermore, we previously reported that PA28γ is responsible
324 for the core protein-related pathological changes. The PA28 family members, namely,
325 α, β and γ, form heptamers that bind to the 20S proteasome and then stimulate
326 polyubiquitin-independent proteasome activity. The PA28γ homoheptamer activates the
327 20S CP for the degradation of PA28γ-binding proteins. In mice, HCV core protein
328 expression induces the development of hepatic steatosis, HCC and type II diabetes
329 mellitus (5, 9, 23), which are highly prevalent in hepatitis C patients (35), and these core
330 protein-related pathological conditions are reversed by PA28γ knockout in mice (22,
331 23). The data presented in our previous study also suggest that PA28γ binds the core
332 protein and then induces the degradation of the unfolded core protein to promote viral
333 particle production (20, 21). However, the mechanism by which the core protein
334 induces HCV-related pathological changes via a PA28γ-related pathway remains
335 unknown. In this study, the results of the yeast two-hybrid screen using PA28γ as bait
336 revealed that RNF1 and RNF2 were the candidate PA28γ-binding partners. PA28γ
337 bound both RNF1 and RNF2 (Fig. 1) and accelerated RNF2 degradation but only
338 weakly affected RNF1 degradation, leading to the upregulation of HOX gene
339 expression (Figs. 2 to 5). Furthermore, PA28γ promoted the proteasome-dependent
340 degradation of RNF2 to impair the monoubiquitination of histone H2A (Figs. 4 to 6).
341 Liu et al reported that CBP-induced acetylation of PA28γ at K195 resulted in
342 homoheptamerization of PA28γ and subsequently stimulated polyubiquitin-independent
343 proteasome activity (32). The data shown in Figs. 8 and 9 support the idea that CBP-
344 dependent acetylation of PA28γ leads to heptamerization of PA28γ (Fig. 8) and suggest
345 that core protein expression promotes the acetylation of PA28γ via CBP activity in
346 infected cells (Fig. 9). Taken together, these data suggest that after HCV infection, the
347 core protein reinforces the interaction between CBP and PA28γ, induces PA28γ
348 heptamerization, and subsequently stimulates polyubiquitin-independent proteasome
349 activity for RNF2 protein degradation. The data presented in this study also suggest that
350 PA28γ expression is required for the reduction in H2Aub in HCV-infected cells.
351 Identifying the other loci and genomic regions at which PA28γ reduces the level of
352 H2Aub is an important and challenging task necessary for understanding the
353 physiological and pathological functions of PA28γ in hepatitis C pathogenesis. A model
354 of the mechanism by which HCV infection facilitates the degradation of RNF2 via a

355 PA28γ-dependent proteasome pathway to impair histone H2A monoubiquitination and
356 induce HOX gene expression is shown in Fig. 10.
357 Several reports indicate that the core protein promotes the degradation of p21
358 (36, 37), whereas other reports suggest that the core protein induces G1 arrest after
359 common bile duct ligation, alters the cell cycle in hepatocytes and is associated with
360 increased p21 expression (38). PA28γ was reported to bind cyclin kinase inhibitors,
361 such as p21 and p19, to promote their degradation via the PA28γ-20S CP complex and
362 then to induce S phase entry (18, 39). These observations and the data presented in the
363 current study suggest that the core protein may regulate the cell cycle via the control of
364 the PA28γ-dependent proteasome. In addition, HOX protein expression induced by the
365 core protein may promote the transcriptional activation of genes associated with
366 degradation of cell cycle inhibitors. HOXA10 overexpression was reported to promote
367 the expression of S-phase kinase-associated protein 2 (SKP2), which contributes to the
368 degradation of the cell cycle inhibitor p27 (40). The upregulation of HOX gene
369 expression in HCV-infected hepatocytes may be associated with the promotion of cell
370 cycle progression via transcriptional and/or posttranslational regulation of cell cycle
371 inhibitors.
372 The induction of HOX genes may contribute to carcinogenesis by regulating
373 cell growth, survival, migration and invasion in addition to regulating the cell cycle.
374 Several HOX genes have been reported to be dysregulated in a tissue-specific manner.
375 HOXB13 is upregulated in breast cancer, whereas its expression is suppressed in
376 prostate cancer (41, 42). HOXD10 is upregulated in breast, gastric, hepatocellular,
377 colorectal, bladder and prostate cancers (43). HOXA9 is upregulated in acute
378 lymphocytic leukaemia and epigenetically silenced in lung cancers (44, 45). HOXA5,
379 HOXA7, HOXA13 and HOXD3 are highly expressed in HCC tissues compared to
380 normal tissues (46). Notably, HOXA13 and HOTTIP were found to be highly expressed
381 in the same neoplastic hepatocyte populations and in liver cancer cell lines (46, 47).
382 HOTTIP, a long noncoding RNA (lncRNA) located contiguous to the HOXA13 gene,
383 directly interacts with WDR5/MLL complexes to induce an open chromatin
384 configuration by driving histone H3 Lys 4 trimethylation, leading to the induction of
385 HOXA genes, including HOXA13 (48); moreover, HOXA13 can induce the
386 transcription of HOTTIP as well as genes related to cell growth and cell invasion (47,
387 49). High expression of both HOTTIP and HOXA13 was correlated with metastasis

388 formation and poor patient survival in HCC, suggesting that HOTTIP/HOXA13
389 expression may be a possible marker for predicting clinical outcomes in HCC patients
390 (47). Although HCV infection cannot potently induce HOXA13 gene transcription in
391 Huh7OK1 cells (10), the discrepancies in the data between our previous study and the
392 abovementioned *in vivo* study may be due to the high expression of HOXA13/HOTTIP
393 in the Huh7 cell line, regardless of the HCV infection status (47). Another lncRNA,
394 HOTAIRM1, was also reported to induce the expression of HOXA1, which could
395 promote the expression of Nanog (50). Some HOX genes associated with
396 carcinogenesis may be constitutively expressed via a positive feedback loop in
397 hepatocytes after DAA treatment.
398 In this study, HCV infection reduced the level of RNF2 and reactivated the
399 expression of silenced HOX genes. However, some clinical reports suggest that the
400 RNF2 and HOX proteins are highly expressed in cancer tissues (51). The data presented
401 in this study may reflect the status of HCV-infected hepatocytes during the early stage
402 and before the premalignant state of liver cancer but not during the malignant state of
403 liver cancer. The expression of some HOX genes has been reported to be maintained in
404 the malignant state of HCC regardless of the high expression of PRC1 components,
405 including RNF2 and PCGF4 (BMI1), suggesting that the expression of some HOX
406 genes may be regulated by factors other than PRC1, such as lncRNAs (e.g., HOTTIP,
407 described above), regardless of the high RNF2 activity at the malignant stage of HCC.
408 Increased expression of RNF2 in HCC tissue was reported to synergistically regulate
409 crosstalk among the histone modifications H2Aub, H3K27me3 and H3Kme3 to
410 suppress E-cadherin transcription (52). HCV infection increases the RNF2 mRNA level
411 but reduces the RNF2 protein level in HCV-infected hepatocytes (10) and may
412 subsequently irreversibly trigger RNF2 transcription, which may be maintained even
413 after viral eradication at the malignant stage of HCC.
414 The possibility remains that PA28γ activation in HCV-infected cells may be
415 associated with viral particle production in these cells. The data presented in our early
416 work revealed that PA28γ knockdown reduced the production of HCV viral particles in
417 the supernatant but did not affect viral RNA replication (21). In this study, compared
418 with that in wild-type cells, the core protein level was much higher in either infected or
419 core protein-expressing PA28γ-knockout cells (Fig. 6A, 7A), while PA28γ knockout
420 reduced the infectious titre in the culture supernatant but did not affect viral RNA

421 replication (Fig. 6C). Nonfunctional or unfolded core proteins were reported to interact
422 with PA28γ for their proteasome-dependent degradation (20, 53). A functional core
423 protein may be engulfed by a nonfunctional or an unfolded core protein in the absence
424 of PA28γ to suppress viral particle production. Alternatively, a reduction in PRC1
425 activity may affect the expression of host genes related to membrane trafficking or viral
426 assembly. Further study is required to clarify the mechanism by which depletion of
427 PA28γ reduces the production of infectious HCV particles.
428 An increasing number of studies have suggested that the PA28γ proteasome is
429 associated with several kinds of viral infections. Coxsackievirus B3 infection was found
430 to promote PA28γ-mediated proteolysis of p53 (54), suggesting that p53 degradation
431 increases viral replication by reducing the inhibitory influence of p53 on viral
432 replication. On the other hand, PA28γ-dependent proteasome activity was associated
433 with an inhibitory effect on viral replication. Ko et al reported that PA28γ acted as a
434 corepressor of human T-lymphotropic virus 1 (HTLV-1) p30 and was required for the
435 suppression of viral replication and maintenance of viral latency (55). Regarding
436 hepatitis B virus (HBV) infection, PA28γ was reported to be associated with HBV
437 pathogenesis. The HBV X protein (HBx) activates HBV promoters to increase HBV
438 RNA transcription, increase the abundance of covalently closed circular DNA
439 (cccDNA) and promote the degradation of the host protein Smc5/6, which can inhibit
440 HBV replication (56, 57). HBx plays an important oncogenic role in the liver in
441 hepatitis B patients (58). For example, HBx promotes the expression of PA28γ to
442 degrade p16 to promote progression through the G1 and M phases (59). In addition,
443 PA28γ stabilizes the HBx protein by competitively inhibiting the binding of HBx to
444 Siah-1 (60). HBx was reported to be polyubiquitinated by Siah-1 for proteasome-
445 dependent degradation (61), and PA28γ competitively inhibited the binding of Siah-1 to
446 HBx, leading to an increase in HBx stability. Thus, PA28γ may be an attractive target
447 for the treatment of hepatitis B and C as well as other viral diseases.
448 In summary, our data presented herein indicate that HCV infection or core protein
449 expression reinforces the interaction between CBP and PA28γ and promotes PA28γ
450 acetylation and heptamerization to activate the proteasome for RNF2 degradation and
451 that a reduction in the RNF2 protein level impairs the monoubiquitination of histone
452 H2A at K119 in the promoter regions of HOX alleles. The reactivation of silenced HOX
453 genes may be associated with HCV-related hepatocellular carcinogenesis. PRC1-

454 dependent histone H2A monoubiquitination silences non-HOX genes (62) and
455 positively or negatively regulates metabolic and developmental gene expression in
456 association with RNA polymerase (63). HCV infection may lead to regulatory effects
457 on various genes via the PCR1-H2Aub pathway during acute and/or chronic infection.
458 Thus, elucidating the mechanism by which HCV infection can regulate PRC1 activity to
459 regulate genes other than HOX genes is important for clarifying the molecular
460 mechanism of hepatitis C pathogenesis and for the development of therapies for
461 hepatitis C.
462

463 **MATERIALS AND METHODS**

464 ***Cell lines, HCV strain.***

465 The HCV strain JFH-1, which belongs to genotype 2a (64), was used as the cell culture-
466 adapted HCV (HCVcc) strain in this study. The viral RNA encoded in the plasmid
467 pJFH1 was transcribed and introduced into Huh7 OK1 cells according to the method
468 reported by Wakita et al. (64). The cell infection procedure was reported previously (10)
469 and is described in detail in each figure legend. The Huh7 OK1 cell line, a subclone
470 derived from Huh-7 cells that is highly permissive to infection with the JFH-1 strain,
471 was cultured as reported previously (65). The human embryonic kidney 293T cell line
472 was purchased from the American Type Culture Collection (Manassas, VA, USA). The
473 lysine deacetylase inhibitor TSA and KAT inhibitor C646 were purchased from Sigma–
474 Aldrich Japan (Tokyo, Japan).
475

476 **Plasmids.**

477 The gene encoding PA28γ was subcloned and inserted into the pGBKT7 vector
478 (resulting in the pGBKT7PA28γ plasmid). N-terminal HA-tagged RNF1 or RNF2 was
479 amplified by polymerase chain reaction (PCR) from human liver cDNA using *KOD*
480 DNA polymerase (TOYOBO, Osaka, Japan) and was then inserted into pCAGGS-PM3.
481 The DNA fragment encoding PA28γ was cloned and inserted into pEF pGKpuro and
482 pEF FLAG Gs pGKpuro as reported previously, with the resulting plasmids designated
483 pEF PA28γ and pEF FLAG-PA28γ, respectively (21), as well as into pEGFP-C3
484 (Clontech Takara, Tokyo, Japan). The plasmid encoding the HCV core protein (amino
485 acids 1-192) was used for cloning and insertion of the corresponding DNA into
486 pCAGGS-PM3 as described previously, and the resulting plasmid was designated

487 pCAG-Core (21). N-terminal FLAG-tagged CBP/p300 cDNA was amplified by PCR
488 and was then inserted into pcDNA3.1 (Invitrogen Thermo, Carlsbad, CA).
489
490 ***Yeast two-hybrid screening.***
491 The bait plasmid pGBKT7PA28γ was introduced into *Saccharomyces*
492 *cerevisiae* AH109 cells. Yeast cells containing pGBKT7PA28γ were grown in yeast
493 extract-peptone-dextrose medium and transfected with a human foetal brain plasmid
494 library based on pACT2 (Clontech Takara). Clones (22.4×10^6) generated with the
495 library were screened (Clontech Takara, Tokyo, Japan). Yeast clones containing
496 pGBKT7-53 and pGADT7-T (Clontech) were used as positive controls, while yeast
497 clones containing pGBKT7 and pGADT7 were used as negative controls. Yeast
498 colonies grown on dropout plates lacking tryptophan, leucine, histidine, and adenine
499 were inoculated on two fresh dropout plates lacking leucine and tryptophan. One of the
500 two plates was used for a β-galactosidase assay according to the method of Duttweiller
501 (66), and the other plate was stored at 4 °C as a master plate. One of the 556 dropout
502 plate-positive clones exhibited dark blue staining on a β-galactosidase assay plate to the
503 same extent as the positive control and was called C1-26. The plasmid in Cl-26 cells
504 encoded the RNF1 gene. We amplified the genes encoding RNF1 and the RNF1
505 homologue RNF2 from the total human liver cDNA by PCR and then inserted the
506 sequences into several plasmids as described above. We also isolated the yeast clone
507 encoding PA28γ by this screening method, which supported the accuracy of this
508 screening method.
509
510 ***Transfection, immunoblotting, immunoprecipitation, and gene silencing.***
511 Plasmid DNA was transfected into Huh7OK1 or 293T cells by using TransIT®-LT1
512 (Mirus Bio, Madison, WI). Lysate preparation and immunoprecipitation were carried
513 out as described previously (21). The cell lysates were subjected to 5-20% sodium
514 dodecyl sulfate–polyacrylamide gel electrophoresis (SDS–PAGE) for standard protein
515 analysis or to native PAGE using a NativePAGE™ 3–12% mini protein gel and a
516 Sample Prep Kit (Thermo Fisher) for analysis of the heptamerization of PA28γ. The
517 proteins in the gel were transferred onto polyvinylidene difluoride membranes (Merck
518 Millipore, Billerica, MA). After protein transfer, the membranes were incubated first
519 with an appropriate primary antibody and then with a horseradish peroxidase-

520 conjugated rabbit or mouse IgG as a secondary antibody, immersed in Super Signal
521 West Femto (Thermo Fisher Scientific, Rockford, IL) and visualized using an LAS
522 4000 Mini imaging system (Cytiva, Marlborough, MA). The small interfering RNAs
523 (siRNAs) targeting RNF2 and the control siRNA (siControl Non-targeting siRNA #2,
524 Dharmacon®) were purchased from Thermo Scientific (Brebières, France) and were
525 introduced into cells by using Lipofectamine RNAiMax (Thermo Fisher Scientific). The
526 Silencer® siRNAs with ID numbers s3495 and s3497 were purchased from Thermo
527 Fisher Scientific and are designated CBP#1 and siCBP#2, respectively, in this study.
528 The CHX chase assay was carried out by the method reported by Kao et al (67).
529
530 ***Reverse transcription–quantitative polymerase chain reaction (RT–qPCR) and***
531 ***reverse transcription–semiquantitative polymerase chain reaction (RT–sqPCR).***
532 Total RNA and first-strand cDNA were prepared and then evaluated by RT–qPCR as
533 described previously (10). The expression levels of HCV RNA and of each host mRNA
534 were normalized to that of GAPDH mRNA. HCV RNA and GAPDH mRNA were
535 amplified using primer pairs as described previously (21, 65). Each PCR product was
536 confirmed to be detected as a single band of the correct size by agarose gel
537 electrophoresis. The amount of HCV in the culture supernatant was estimated as the
538 copy number (10). HOX gene mRNA levels were measured by RT–sqPCR or RT–
539 qPCR (68) using the appropriate primer pairs as described previously (10). Takara
540 Emerald (2x;Takara Co.) was used for RT–sqPCR. Data acquisition was performed for
541 25, 30, 35, and 40 cycles to confirm that the plateau phase had not been reached.
542
543 ***Evaluation of immunofluorescence staining in cells by microscopy.***
544 Huh7OK1 wild-type or transfected cells were infected with HCVcc, passaged twice
545 every 4 days, seeded at 0.5×10^4 cells per well on a glass cover slip and incubated at
546 37 °C for 24 h. The cells were washed twice with phosphate-buffered saline (PBS) and
547 fixed with 4% paraformaldehyde at room temperature for 20 min. After fixation, the
548 cells were washed twice with PBS, permeabilized by incubation for 15 min at room
549 temperature in PBS containing 0.3% saponin, and then incubated in PBS containing 3%
550 bovine serum albumin (PBS-BSA) to block nonspecific signals. These cells were
551 stained with 50 μM 4',6-diamidino-2-phenylindole (DAPI) and incubated at 4 °C
552 overnight in PBS-BSA containing rabbit anti-RNF2 IgG (clone D22F2, Cell Signaling

553 Technology, Denver, MA) and mouse anti-NS5A IgG (clone 9E10) or rabbit anti-
554 H2Aub IgG (clone D27C4, Cell Signaling Technology) and mouse anti-HCV core
555 protein IgG (clone B2, ANOGEN, Mississauga, Canada). The cells were washed three
556 times with PBS-BSA and incubated at room temperature for 2 h in PBS-BSA
557 containing appropriate Alexa Fluor (AF)488 or AF594-conjugated secondary antibodies
558 (Thermo Fisher Scientific). The cells were washed three times with PBS-BSA and
559 observed using a confocal laser scanning microscope (FV1000, Olympus, Tokyo) or
560 fluorescence microscope (BZ-9000 and BZ-X800: Keyence, Osaka, Japan).
561 After reacting with each the first antibody, PA28γ and RNF2 were detected using
562 AF488- and AF594-conjugated secondary antibodies, respectively. Nuclei were stained
563 with DAPI. Localization signals of PA28γ and RNF2 were obtained as three-
564 dimensional (Fig. 1C) and two-dimensional images (Figs. 1B and 4B) using all-in-one
565 fluorescence microscope (BZ-X800, KEYENCE, Osaka, Japan) equipped with a Plan
566 Apochromat 40x objective (NA0.95, BZ-PA40, KEYENCE, Osaka, Japan) and optical
567 sectioning module (BZ-H4XF, KEYENCE, Osaka, Japan). Green fluorescence was
568 detected using a GFP filter (ex:470/40nm, em:525/50nm, dichroic:495nm, OP-87763,
569 KEYENCE, Osaka, Japan), while red fluorescence was detected using a Texas Red
570 filter (ex:560/40nm, em:630/75nm, dichroic:585nm, OP-87765, KEYENCE, Osaka,
571 Japan). Blue fluorescence was detected using a DAPI filter (ex:360/40nm,
572 em:460/50nm, dichroic:400nm, OP-87762, KEYENCE, Osaka, Japan). Images were
573 acquired as continuous images using the sectioning function. Fluorescence was
574 measured for the image at the center depth of the Z-axis of the acquired serial images,
575 and each signal intensity of the same coordinate pixel within the DAPI-positive region
576 (nuclear region) was compared and evaluated using a fluorescence microscope and the
577 corresponding software (BZ-H4: Keyence, Osaka, Japan). Co-localization of PA28γ
578 and RNF2 (Fig. 4B) was determined using the function evaluating co-localization
579 included in a confocal laser microscope FV1000.
580
581 ***ChIP assay.***
582 ChIP assays were carried out according to the method reported by Sakurai et al (69)
583 with modifications as described previously (10). Huh7OK1 cells were infected with
584 HCVcc and passaged twice every 4 days. HCV-infected cells and mock-infected cells

585 were harvested 8 dpi. DNA–protein complexes were prepared as described previously
586 (10). qPCR was carried out as described above without a reverse transcription step.
587
588 ***Gene knockout with the CRISPR/Cas9 system.***
589 PA28γ-knockout Huh7OK1 cell lines were established according to the method
590 reported by Fujihara et al. (70). A PA28γ-targeting sequence (5'-
591 ATGGGATGCTGAAAAGCAAC -3'), which is located in the exon 5, was used for the
592 construction of the pX330 plasmid encoding the guide RNA. The targeted DNA regions
593 were amplified from the genomic DNA of Huh7OK1 cells with the primer pair 5'-
594 ACTGAGGATCCATGTTTTAGACGCTCATCTGTAGTTC-3'/5'-
595 GATATCGAATTCCAACCCAGGAGGCAGAGGTC-3' and were subsequently
596 inserted into pCAG EGxxFP. Both pX330 and pCAG EGxxFP were purchased from
597 Addgene (Cat Nos. #42230 and #50716; Cambridge, MA). Huh7OK1 cells were
598 transfected with these plasmids using Lipofectamine LTX (Thermo Fisher Scientific).
599 GFP-positive cells were isolated using a FACSAria^{TM} cell sorter (BD Bioscience) 48 h
600 post-transfection. Single-cell clones were established by a colony isolation technique.
601 The deleted regions of each allele of the PA28γ gene were confirmed by direct
602 sequencing. The PA28γ mRNA transcribed from each allele in the PA28γ-knockout cell
603 line lacked the sequence 5'-GCTGAAAAGCAACCAGCAGC or ACCAGCAGCTG-
604 3', corresponding to the region on the downstream of amino acid residue 7 or 3. The
605 expression of PA28γ was confirmed by immunoblot analysis and direct sequencing.
606 There appears to be no difference between wild-type and knockout cells with respect to
607 cell proliferation.
608
609 ***In vitro proteasome assay***
610 The plasmids encoding HA-RNF1 and HA-RNF2 were transfected into PA28γ-
611 knockout Huh7OK1 cells (5 x 10^5 cells) and then harvested 48 hr. The cell lysates were
612 prepared in 1 ml of NP-40 Lysis buffer (50 mM Tris 7.4 pH, 150 mM NaCl, 1% NP-40,
613 10% glycerol, 1x protease inhibitor cocktail). HA-RNF1 or HA-RNF2 was then isolated
614 by immunoprecipitation using an anti-HA antibody for *in vitro* proteasome assays.
615 The in vitro proteasome assay was conducted using purified 20S proteasome (Enzo Life
616 Science, Farmingdale, NY) and proteasome activator 11S γ subunit (Enzo Life
617 Science). The immunoprecipitates containing HA-RNF1 or HA-RNF2 (one-twentieth of

618 the total immunoloprecipitates) were mixed on ice with 20S CP (50 ng protein) with or
619 without the 11S PA consisting of PA28γ (28 ng protein) in proteasome assay buffer (25
620 mM Tris-HCl pH7.4, 10% glycerol, 10 mM $MgCl_2$, 1 mM DTT, 2 mM ATP). The
621 mixture was incubated at 37 ˚C and stopped at 0, 10 or 30 min by boiling after adding
622 SDS-sample buffer. The resulting mixtures were analysed by Western blotting. Intensity
623 of RNF1 and RNF2 protein signals were measured using Image Gauge software (GE
624 health care).
625
626 ***Statistical analysis.***
627 The measured values are shown as the means ± standard deviations (SDs). Normality
628 tests were performed by the Shapiro-Lorc test and Q-Q plots. Correlation tests were
629 performed by Pearson's correlation test for samples that showed a normal distribution,
630 and by Spearman's rank correlation test for the others. The statistical significance of
631 differences in the means was determined by Student's *t* test. A *p*-value less than 0.05
632 was considered statistically significant (*: $p < 0.05$, **: $p < 0.01$).
633
634 **Acknowledgements**
635 We thank T. Wakita, F. V. Chisari and R. Bartenschlager for providing plasmids and
636 cell lines. We also thank M. Mori for her secretarial work and C. Endoh for technical
637 assistance. This work was supported by Grants-in-Aid from the Japan Agency for
638 Medical Research and Development (24fk0210109), JST Moonshot R&D
639 (JPMJMS2025), and scholarship donations from Teijin Co. Ltd and Yakult Co., Ltd.
640

641 **Figure legends.**

642 **FIG 1: PA28γ could bind RNF2 but was not colocalized with RNF2.**

643 (A) FLAG-PA28γ was expressed in 293T cells together with HA-RNF1 or HA-RNF2.
644 The cells were harvested 48 h post-transfection. These cell lysates were subjected to
645 immunoprecipitation. Immunoprecipitates recovered with anti-HA or anti-FLAG
646 antibodies were analysed by Western blotting using anti-FLAG or anti-HA antibodies,
647 respectively. (B) The intracellular localization of PA28γ and RNF2 was examined by
648 immunocytofluorescence. Images were acquired with a Keyence fluorescence
649 microscope. White bars indicate 5 μm scale. (C) The image in the field of view shown
650 in the top of panel C was acquired with a fluorescence microscope and subjected to
651 three-dimensional reconstruction. The green and red fluorescence intensities in each
652 pixel (in coordinate form) were calculated using the analysis software. Pearson's
653 correlation test was performed, and the correlation coefficient (R) was calculated. The
654 data shown in this figure are representative of three independent experiments.

655

656 **FIG 2. The endogenous RNF2 protein was stabilized by genetic knockout of**
657 **PA28γ.**

658 (A) PA28γ gene knockout was conducted using the Huh7OK1 cell line and the
659 CRISPR-Cas9 system. PA28γ was detected in the parental cells but not in the PA28γ-
660 knockout cells. PA28γ-knockout Huh7OK1 cells or parental Huh7OK1 cells
661 (Huh7OK1) were treated with the translation inhibitor CHX (2 mg/ml). Endogenous
662 RNF1, RNF2 and BMI1 expression was evaluated by Western blotting. (B) The band
663 densities of RNF1, RNF2, BMI1 and β-actin shown in panel A were estimated using
664 ImageJ software. The values for RNF1, RNF2 and BMI1 were normalized to that of β-
665 actin and are presented as percentages with respect to those in mock-infected cells. The
666 p-value of each time measurement of KO cell line compared to that of WT cell line
667 were lower than 0.01. The p-values of 2, 4, and 6 h measurements compared to 0 h
668 measurement indicated 0.07, 0.02, and 0.01, respectively (the middle graph), suggesting
669 that RNF2 was decreased in WT cells in a time-dependent manner. The data shown in
670 this figure are representative of three independent experiments and are presented as the
671 means ± SDs (n = 3). **: $p < 0.01$.

672

673 **FIG 3. RNF2 degradation was promoted by the expression of PA28γ.**

674 (A) PA28γ-knockout Huh7OK1 cells were transfected with pEF PA28γ (0, 0.03, 0.1
675 and 0.3 μg/sample) or the empty vector. The total amount of transfected DNA in pEF
676 PA28γ-transfected cells was supplemented with the empty plasmid to a final amount of
677 0.3 μg per sample. Endogenous RNF1, RNF2, BMI1, PA28γ and β-actin expression
678 was evaluated by Western blotting. (B) Total RNA was prepared from the harvested
679 cells described in panel A. The levels of RNF1 mRNA and RNF2 mRNA were
680 estimated via RT–qPCR. These mRNA levels were normalized to the GAPDH mRNA
681 level and are presented as relative values compared to the empty plasmid control. The
682 data shown in this figure are representative of three independent experiments and are
683 presented as the means ± SDs (n =3). (C) PA28γ-knockout Huh7OK1 cells were
684 transfected with pEF PA28γ (0, 0.03, 0.1 and 0.3 μg/sample) or the empty vector
685 together with the plasmid encoding HA-RNF1 or HA-RNF2 (0.2 μg/sample). The total
686 amount of transfected DNA in pEF PA28γ-transfected cells was supplemented with the
687 empty plasmid to a final amount of 0.5 μg per sample. (D) The immuno-precipitates
688 including HA-RNF1 or HA-RNF2 were mixed with 20S CP and 11S PA (PA28γ) in the
689 reaction buffer and then incubated at 0, 10 or 30 min. The resulting preparations were
690 subjected into Western blotting. The data shown in this figure are representative of three
691 independent experiments.
692
693 **FIG 4. The degradation of the RNF2 protein and the reduction in H2Aub were**
694 **promoted by PA28γ and suppressed by proteasome inhibition.**
695 (A) PA28γ-knockout Huh7OK1 cells were transfected with pEF PA28γ and treated with
696 10 μM MG132 at 48 h post-transfection. The resulting cells were harvested at 52 h post-
697 transfection. These cell lysates were subjected to Western blotting. (B) The cells
698 described in panel A were fixed and stained with the appropriate antibodies as described
699 in the Materials and Methods. The intracellular localization of RNF2 and PA28γ was
700 observed via confocal laser scanning microscopy. White bars in high magnified images
701 (2 panels on right side) indicate 5 μm scale, while those in other panels indicated 10 μm
702 scale. (C) PA28γ-knockout cells were transfected with plasmids encoding PA28γ or
703 PA28γP245Y. The resulting cells were fixed 48 h post-transfection and stained with
704 appropriate antibodies as described in the Materials and Methods. The nuclear
705 localization of RNF2 and PA28γ was observed via Keyence fluorescence microscope.
706 White bars indicate 5 μm scale. The green and red fluorescence intensities in each pixel

707 (in coordinate form) were calculated using the analysis software. Spearman's rank
708 correlation test was performed. Each correlation coefficient (R) was shown.
709 The data shown in this figure are representative of three independent experiments.
710
711 **FIG 5. PA28γ was required for the induction of HOX genes.**
712 (A) PA28γ-knockout Huh7OK1 cells were transfected with pEF PA28γ (0, 0.1, 0.3 and
713 1.0 μg/sample) or the empty vector. The total amount of transfected DNA in these cells
714 was supplemented with the empty plasmid to a final amount of 1.0 μg per sample.
715 These cells were treated with 10 μM MG132 at 48 h post-transfection and were then
716 harvested at 52 h post-transfection. These cell lysates were subjected to Western
717 blotting. (B and D) Total RNA was prepared from the harvested cells described in panel
718 A. The level of each HOX mRNA was estimated via RT–qPCR. These mRNA levels
719 were normalized to the GAPDH mRNA level and are presented as relative values
720 compared to the empty plasmid control. The data shown in this figure are representative
721 of three independent experiments and are presented as the means ± SDs (n =3). (C) The
722 level of H2Aub in the promoter region of HOXB9 was evaluated by a chromatin
723 immunoprecipitation (ChIP) assay. The data shown in this figure are representative of
724 three independent experiments and are presented as the means ± SDs (n =3).
725
726 **FIG 6. HCV infection reduced the levels of H2Aub and RNF2 in the presence but**
727 **not in the absence of PA28γ.**
728 Huh7OK1 cells (WT) and PA28γ-knockout Huh7OK1 cells (PA28γKO) were infected
729 with HCVcc at m.o.i. of 0.5 and harvested at 0, 3 and 6 dpi. These cell lysates were
730 subjected to Western blotting (A), and the band densities of H2Aub and RNF2 were
731 estimated by a method similar to that described in Figs. 2 and 5 (B). The levels of
732 cellular and supernatant HCV RNA were estimated by RT–qPCR, and the infectivity in
733 the supernatant was estimated by a focus formation assay (C). The data shown in this
734 figure are representative of three independent experiments and are presented as the
735 means ± SDs (n =3).
736
737 **FIG 7. HCV core protein expression reduced the levels of H2Aub and RNF2 in the**
738 **presence but not in the absence of PA28γ.**

739 (A) PA28γ-knockout Huh7OK1 cells (PA28γKO) and the parental cells (WT) were
740 transfected with pCAG Core (0, 0.1, 0.3 and 1.0 μg/sample) or the empty vector. The
741 total amount of transfected DNA in these cells was supplemented with the empty
742 plasmid to a final amount of 1.0 μg per sample. These cell lysates were subjected to
743 Western blotting. The data shown in this figure are representative of three independent
744 experiments. (B) The cells described in panel A were subjected to a ChIP assay to
745 estimate the level of H2Aub in the promoter region of HOXB9. The data shown in this
746 figure are representative of three independent experiments and are presented as the
747 means ± SDs (n =3). (C) Total RNA was prepared from the cells described in panel A.
748 The level of HOXB9 mRNA was estimated by RT–qPCR. The data shown in this figure
749 are representative of three independent experiments and are presented as the
750 means ± SDs (n =3).
751
752 **FIG 8: Acetylation of PA28γ at K195 was essential for the reduction in the RNF2**
753 **protein level.**
754 (A and B) PA28γ-knockout HuhOK1 cells were transfected with pEF PA28γ or the
755 empty vector and were then treated with C646 and CHX at 36 h post-transfection. The
756 cells were collected at 42 h post-transfection. These cell lysates were subjected to
757 Western blotting. (C and D) PA28γ-knockout HuhOK1 cells were transfected with pEF
758 PA28γ or the empty vector and were then treated with TSA at 36 h post-transfection.
759 The cells were collected at 0, 2 and 4 h posttreatment. These cell lysates were subjected
760 to Western blotting. (E) PA28γ, PA28γ K195R or PA28γK195Q were expressed in
761 PA28γ-knockout Huh7OK1 cells. The transfected cells were treated with CHX and
762 harvested at 0, 2 and 6 h posttreatment. These cell lysates were subjected to Western
763 blotting. (F) Huh7OK1 cells were transfected with pCAG Core (0, 0.3 and 1.0
764 μg/sample) or the empty vector. The total amount of transfected DNA in these cells was
765 supplemented with the empty plasmid to a final amount of 1.0 μg per sample. The cells
766 were treated with CHX at 36 h post-transfection and harvested at 42 h post-transfection.
767 These cell lysates were subjected to Western blotting.
768
769 **FIG 9. HCV core proteins induce the acetylation and activation of PA28γ via the**
770 **KAT CBP, leading to a decrease in the RNF2 protein level.**

771 (A) Parental Huh7OK1 cells and PA28γ-knockout Huh7OK1 cells were infected with
772 HCVcc at an m.o.i. of 0.5 and harvested at 0, 3 and 6 dpi. These cell lysates were
773 subjected to immunoprecipitation using rabbit anti-Ace-K IgG or normal rabbit IgG.
774 The resulting precipitates and cell lysates were subjected to Western blotting. (B) The
775 cell lysates described in panel A were subjected to Western blotting to analyse the
776 formation of PA28γ heptamers. (C) PA28γ-knockout Huh7OK1 cells were transfected
777 with pEF PA28γ (0.3 μg/sample) and/or pCAG Core (0.3 μg/sample). Total DNA was
778 supplemented with the empty plasmid to a final amount of 1.0 μg per sample. The cells
779 were harvested at 48 h post-transfection. These cell lysates were subjected to
780 immunoprecipitation using rabbit anti-Ace-K IgG or normal rabbit IgG. The resulting
781 precipitates and cell lysates were subjected to Western blotting. (D) The cell lysates
782 described in panel C were subjected to Western blotting to analyse the formation of
783 PA28γ heptamers. (E) PA28γ-knockout Huh7OK1 cells were transfected with pEGFP
784 PA28γ (0.3 μg/sample), pcDNA3.1 FLAG-CBP (0.3 μg/sample), and/or pCAG Core
785 (0.3 μg/sample). Total DNA was supplemented with the empty plasmid to a final
786 amount of 1.0 μg per sample. The cells were harvested at 48 h post-transfection. The
787 resulting cell lysates were subjected to immunoprecipitation and Western blotting. (E)
788 Huh7OK1 cells were transfected with control siRNA (c), siCBP#1 (#1) or siCBP#2
789 (#2). The transfected cells were infected at 16 h post-transfection with HCVcc at an
790 m.o.i. of 0.5. The infected cells were harvested at 3 dpi. The resulting cell lysates were
791 subjected to Western blotting.
792
793 **FIG 10. Schematic diagram of the mechanism by which HCV infection**
794 **accelerates the activation of the PA28γ-20S CP complex for the degradation of**
795 **RNF2, the reduction in H2Aub, and the induction of HOX genes.**
796 Most HOX alleles are silenced in uninfected hepatocytes (10). When hepatocytes are
797 infected with HCV, the core protein reinforces the interaction between CBP and PA28γ
798 to increase PA28γ acetylation and heptamerization. The PA28γ heptamer recruits RNF2
799 and activates the 20S CP to degrade RNF2. The degradation of RNF2 results in a
800 decrease in PRC1 activity and impairs the monoubiquitination of histone H2A. The
801 reduction in H2Aub results in the formation of open chromatin in the promoter regions
802 of HOX alleles and the transcriptional reactivation of silenced HOX genes.
803

804 **REFERENCES**

805

806 1. WHO. 2024. Fact sheet: Hepatitis C, *on* World Health Organization.
807 https://www.who.int/news-room/fact-sheets/detail/hepatitis-c. Accessed
808 2. Marshall AD, Willing AR, Kairouz A, Cunningham EB, Wheeler A, O'Brien N,
809 Perera V, Ward JW, Hiebert L, Degenhardt L, Hajarizadeh B, Colledge S,
810 Hickman M, Jawad D, Lazarus JV, Matthews GV, Scheibe A, Vickerman P,
811 Dore GJ, Grebely J, Global HCV, Group HIVTR. 2024. Direct-acting antiviral
812 therapies for hepatitis C infection: global registration, reimbursement, and
813 restrictions. Lancet Gastroenterol Hepatol 9:366-382.
814 3. Rinaldi L, Nevola R, Franci G, Perrella A, Corvino G, Marrone A, Berretta M,
815 Morone MV, Galdiero M, Giordano M, Adinolfi LE, Sasso FC. 2020. Risk of
816 Hepatocellular Carcinoma after HCV Clearance by Direct-Acting Antivirals
817 Treatment Predictive Factors and Role of Epigenetics. Cancers (Basel) 12.
818 4. Moriishi K. 2017. The potential of signal peptide peptidase as a therapeutic
819 target for hepatitis C. Expert Opin Ther Targets 21:827-836.
820 5. Shintani Y, Fujie H, Miyoshi H, Tsutsumi T, Tsukamoto K, Kimura S, Moriya
821 K, Koike K. 2004. Hepatitis C virus infection and diabetes: direct involvement
822 of the virus in the development of insulin resistance. Gastroenterology 126:840-
823 8.
824 6. Moriya K, Yotsuyanagi H, Shintani Y, Fujie H, Ishibashi K, Matsuura Y,
825 Miyamura T, Koike K. 1997. Hepatitis C virus core protein induces hepatic
826 steatosis in transgenic mice. J Gen Virol 78 (Pt 7):1527-31.
827 7. Roingeard P, Hourioux C. 2008. Hepatitis C virus core protein, lipid droplets
828 and steatosis. J Viral Hepat 15:157-64.
829 8. Mahmoudvand S, Shokri S, Taherkhani R, Farshadpour F. 2019. Hepatitis C
830 virus core protein modulates several signaling pathways involved in
831 hepatocellular carcinoma. World J Gastroenterol 25:42-58.
832 9. Moriya K, Fujie H, Shintani Y, Yotsuyanagi H, Tsutsumi T, Ishibashi K,
833 Matsuura Y, Kimura S, Miyamura T, Koike K. 1998. The core protein of
834 hepatitis C virus induces hepatocellular carcinoma in transgenic mice. Nat Med
835 4:1065-7.

836 10. Kasai H, Mochizuki K, Tanaka T, Yamashita A, Matsuura Y, Moriishi K. 2021.
837 Induction of HOX Genes by Hepatitis C Virus Infection via Impairment of
838 Histone H2A Monoubiquitination. J Virol 95:01784-20.
839 11. Carnesecchi J, Pinto PB, Lohmann I. 2018. Hox transcription factors: an
840 overview of multi-step regulators of gene expression. Int J Dev Biol 62:723-732.
841 12. Feng Y, Zhang T, Wang Y, Xie M, Ji X, Luo X, Huang W, Xia L. 2021.
842 Homeobox Genes in Cancers: From Carcinogenesis to Recent Therapeutic
843 Intervention. Front Oncol 11:770428.
844 13. Wang H, Wang L, Erdjument-Bromage H, Vidal M, Tempst P, Jones RS, Zhang
845 Y. 2004. Role of histone H2A ubiquitination in Polycomb silencing. Nature
846 431:873-8.
847 14. Thomas T, Salcedo-Tacuma D, Smith DM. 2023. Structure, Function, and
848 Allosteric Regulation of the 20S Proteasome by the 11S/PA28 Family of
849 Proteasome Activators. Biomolecules 13.
850 15. Thomas TA, Smith DM. 2022. Proteasome activator 28gamma (PA28gamma)
851 allosterically activates trypsin-like proteolysis by binding to the alpha-ring of the
852 20S proteasome. J Biol Chem 298:102140.
853 16. Li X, Lonard DM, Jung SY, Malovannaya A, Feng Q, Qin J, Tsai SY, Tsai MJ,
854 O'Malley BW. 2006. The SRC-3/AIB1 coactivator is degraded in a ubiquitin-
855 and ATP-independent manner by the REGgamma proteasome. Cell 124:381-92.
856 17. Uchimura Y, Barton LF, Rada C, Neuberger MS. 2011. REG-gamma associates
857 with and modulates the abundance of nuclear activation-induced deaminase. J
858 Exp Med 208:2385-91.
859 18. Chen X, Barton LF, Chi Y, Clurman BE, Roberts JM. 2007. Ubiquitin-
860 independent degradation of cell-cycle inhibitors by the REGgamma proteasome.
861 Mol Cell 26:843-52.
862 19. Paesen GC, Nuttall PA. 1996. A tick homologue of the human Ki nuclear
863 autoantigen. Biochim Biophys Acta 1309:9-13.
864 20. Moriishi K, Okabayashi T, Nakai K, Moriya K, Koike K, Murata S, Chiba T,
865 Tanaka K, Suzuki R, Suzuki T, Miyamura T, Matsuura Y. 2003. Proteasome
866 activator PA28gamma-dependent nuclear retention and degradation of hepatitis
867 C virus core protein. J Virol 77:10237-49.

868 21. Moriishi K, Shoji I, Mori Y, Suzuki R, Suzuki T, Kataoka C, Matsuura Y. 2010.
869 Involvement of PA28gamma in the propagation of hepatitis C virus. Hepatology
870 52:411-20.
871 22. Miyamoto H, Moriishi K, Moriya K, Murata S, Tanaka K, Suzuki T, Miyamura
872 T, Koike K, Matsuura Y. 2007. Involvement of the PA28gamma-dependent
873 pathway in insulin resistance induced by hepatitis C virus core protein. J Virol
874 81:1727-35.
875 23. Moriishi K, Mochizuki R, Moriya K, Miyamoto H, Mori Y, Abe T, Murata S,
876 Tanaka K, Miyamura T, Suzuki T, Koike K, Matsuura Y. 2007. Critical role of
877 PA28gamma in hepatitis C virus-associated steatogenesis and
878 hepatocarcinogenesis. Proc Natl Acad Sci U S A 104:1661-6.
879 24. Murata S, Kawahara H, Tohma S, Yamamoto K, Kasahara M, Nabeshima Y,
880 Tanaka K, Chiba T. 1999. Growth retardation in mice lacking the proteasome
881 activator PA28gamma. J Biol Chem 274:38211-5.
882 25. Huang L, Haratake K, Miyahara H, Chiba T. 2016. Proteasome activators,
883 PA28gamma and PA200, play indispensable roles in male fertility. Sci Rep
884 6:23171.
885 26. Li L, Zhao D, Wei H, Yao L, Dang Y, Amjad A, Xu J, Liu J, Guo L, Li D, Li Z,
886 Zuo D, Zhang Y, Liu J, Huang S, Jia C, Wang L, Wang Y, Xie Y, Luo J, Zhang
887 B, Luo H, Donehower LA, Moses RE, Xiao J, O'Malley BW, Li X. 2013.
888 REGgamma deficiency promotes premature aging via the casein kinase 1
889 pathway. Proc Natl Acad Sci U S A 110:11005-10.
890 27. Okamoto T, Nishimura Y, Ichimura T, Suzuki K, Miyamura T, Suzuki T,
891 Moriishi K, Matsuura Y. 2006. Hepatitis C virus RNA replication is regulated
892 by FKBP8 and Hsp90. EMBO J 25:5015-5025.
893 28. Zhang Z, Clawson A, Realini C, Jensen CC, Knowlton JR, Hill CP, Rechsteiner
894 M. 1998. Identification of an activation region in the proteasome activator
895 REGalpha. Proc Natl Acad Sci U S A 95:2807-11.
896 29. Geng Z, Gao Z. 2020. Mammalian PRC1 Complexes: Compositional
897 Complexity and Diverse Molecular Mechanisms. Int J Mol Sci 21.
898 30. Zhou W, Zhu P, Wang J, Pascual G, Ohgi KA, Lozach J, Glass CK, Rosenfeld
899 MG. 2008. Histone H2A monoubiquitination represses transcription by
900 inhibiting RNA polymerase II transcriptional elongation. Mol Cell 29:69-80.

901 31. Zhu P, Zhou W, Wang J, Puc J, Ohgi KA, Erdjument-Bromage H, Tempst P,
902 Glass CK, Rosenfeld MG. 2007. A histone H2A deubiquitinase complex
903 coordinating histone acetylation and H1 dissociation in transcriptional
904 regulation. Mol Cell 27:609-21.
905 32. Liu J, Wang Y, Li L, Zhou L, Wei H, Zhou Q, Liu J, Wang W, Ji L, Shan P,
906 Wang Y, Yang Y, Jung SY, Zhang P, Wang C, Long W, Zhang B, Li X. 2013.
907 Site-specific acetylation of the proteasome activator REGgamma directs its
908 heptameric structure and functions. J Biol Chem 288:16567-16578.
909 33. Gomez-Gonzalo M, Benedicto I, Carretero M, Lara-Pezzi E, Maldonado-
910 Rodriguez A, Moreno-Otero R, Lai MM, Lopez-Cabrera M. 2004. Hepatitis C
911 virus core protein regulates p300/CBP co-activation function. Possible role in
912 the regulation of NF-AT1 transcriptional activity. Virology 328:120-30.
913 34. Domovitz T, Gal-Tanamy M. 2021. Tracking Down the Epigenetic Footprint of
914 HCV-Induced Hepatocarcinogenesis. J Clin Med 10.
915 35. Chen Y, Ji H, Shao J, Jia Y, Bao Q, Zhu J, Zhang L, Shen Y. 2020. Different
916 Hepatitis C Virus Infection Statuses Show a Significant Risk of Developing
917 Type 2 Diabetes Mellitus: A Network Meta-Analysis. Dig Dis Sci 65:1940-
918 1950.
919 36. Shiu TY, Huang SM, Shih YL, Chu HC, Chang WK, Hsieh TY. 2013. Hepatitis
920 C virus core protein down-regulates p21(Waf1/Cip1) and inhibits curcumin-
921 induced apoptosis through microRNA-345 targeting in human hepatoma cells.
922 PLoS One 8:e61089.
923 37. Chang PC, Chi CW, Chau GY, Li FY, Tsai YH, Wu JC, Wu Lee YH. 2006.
924 DDX3, a DEAD box RNA helicase, is deregulated in hepatitis virus-associated
925 hepatocellular carcinoma and is involved in cell growth control. Oncogene
926 25:1991-2003.
927 38. Chang ML, Chen TH, Chang MY, Yeh CT. 2009. Cell cycle perturbation in the
928 hepatocytes of HCV core transgenic mice following common bile duct ligation
929 is associated with enhanced p21 expression. J Med Virol 81:467-72.
930 39. Li X, Amazit L, Long W, Lonard DM, Monaco JJ, O'Malley BW. 2007.
931 Ubiquitin- and ATP-independent proteolytic turnover of p21 by the
932 REGgamma-proteasome pathway. Mol Cell 26:831-42.

933 40. Gong D, Zhu H, Zeng L, Hu R, Hu J, Ding J. 2021. Overexpression of HOXA10
934 promotes the growth and metastasis of nasopharyngeal carcinoma. Exp Biol
935 Med (Maywood) 246:2454-2462.
936 41. Wang Z, Dahiya S, Provencher H, Muir B, Carney E, Coser K, Shioda T, Ma
937 XJ, Sgroi DC. 2007. The prognostic biomarkers HOXB13, IL17BR, and CHDH
938 are regulated by estrogen in breast cancer. Clin Cancer Res 13:6327-34.
939 42. Jung C, Kim RS, Lee SJ, Wang C, Jeng MH. 2004. HOXB13 homeodomain
940 protein suppresses the growth of prostate cancer cells by the negative regulation
941 of T-cell factor 4. Cancer Res 64:3046-51.
942 43. Surendran H, Palaniyandi T, Natarajan S, Hari R, Viwanathan S, Baskar G,
943 Abdul Wahab MR, Ravi M, Rajendran BK. 2023. Role of homeobox d10 gene
944 targeted signaling pathways in cancers. Pathol Res Pract 248:154643.
945 44. Faber J, Krivtsov AV, Stubbs MC, Wright R, Davis TN, van den Heuvel-
946 Eibrink M, Zwaan CM, Kung AL, Armstrong SA. 2009. HOXA9 is required for
947 survival in human MLL-rearranged acute leukemias. Blood 113:2375-85.
948 45. Rauch T, Wang Z, Zhang X, Zhong X, Wu X, Lau SK, Kernstine KH, Riggs
949 AD, Pfeifer GP. 2007. Homeobox gene methylation in lung cancer studied by
950 genome-wide analysis with a microarray-based methylated CpG island recovery
951 assay. Proc Natl Acad Sci U S A 104:5527-32.
952 46. Cillo C, Schiavo G, Cantile M, Bihl MP, Sorrentino P, Carafa V, M DA,
953 Roncalli M, Sansano S, Vecchione R, Tornillo L, Mori L, De Libero G,
954 Zucman-Rossi J, Terracciano L. 2011. The HOX gene network in hepatocellular
955 carcinoma. Int J Cancer 129:2577-87.
956 47. Quagliata L, Quintavalle C, Lanzafame M, Matter MS, Novello C, di Tommaso
957 L, Pressiani T, Rimassa L, Tornillo L, Roncalli M, Cillo C, Pallante P,
958 Piscuoglio S, Ng CK, Terracciano LM. 2018. High expression of HOXA13
959 correlates with poorly differentiated hepatocellular carcinomas and modulates
960 sorafenib response in in vitro models. Lab Invest 98:95-105.
961 48. Wang KC, Yang YW, Liu B, Sanyal A, Corces-Zimmerman R, Chen Y, Lajoie
962 BR, Protacio A, Flynn RA, Gupta RA, Wysocka J, Lei M, Dekker J, Helms JA,
963 Chang HY. 2011. A long noncoding RNA maintains active chromatin to
964 coordinate homeotic gene expression. Nature 472:120-4.

965 49. Wong CH, Li CH, He Q, Chan SL, Tong JH, To KF, Lin LZ, Chen Y. 2020.
966 Ectopic HOTTIP expression induces noncanonical transactivation pathways to
967 promote growth and invasiveness in pancreatic ductal adenocarcinoma. Cancer
968 Lett 477:1-9.
969 50. Li F, Xu Y, Xu X, Ge S, Zhang F, Zhang H, Fan X. 2020. lncRNA HotairM1
970 Depletion Promotes Self-Renewal of Cancer Stem Cells through HOXA1-
971 Nanog Regulation Loop. Mol Ther Nucleic Acids 22:456-470.
972 51. Yan Q, Chen BJ, Hu S, Qi SL, Li LY, Yang JF, Zhou H, Yang CC, Chen LJ, Du
973 J. 2021. Emerging role of RNF2 in cancer: From bench to bedside. J Cell
974 Physiol 236:5453-5465.
975 52. Yao L, Li J, Jiang B, Zhang Z, Li X, Ouyang X, Xiao Y, Liu G, Wang Z, Zhang
976 G. 2023. RNF2 inhibits E-Cadherin transcription to promote hepatocellular
977 carcinoma metastasis via inducing histone mono-ubiquitination. Cell Death Dis
978 14:261.
979 53. Suzuki R, Moriishi K, Fukuda K, Shirakura M, Ishii K, Shoji I, Wakita T,
980 Miyamura T, Matsuura Y, Suzuki T. 2009. Proteasomal turnover of hepatitis C
981 virus core protein is regulated by two distinct mechanisms: a ubiquitin-
982 dependent mechanism and a ubiquitin-independent but PA28gamma-dependent
983 mechanism. J Virol 83:2389-92.
984 54. Gao G, Wong J, Zhang J, Mao I, Shravah J, Wu Y, Xiao A, Li X, Luo H. 2010.
985 Proteasome activator REGgamma enhances coxsackieviral infection by
986 facilitating p53 degradation. J Virol 84:11056-66.
987 55. Ko NL, Taylor JM, Bellon M, Bai XT, Shevtsov SP, Dundr M, Nicot C. 2013.
988 PA28gamma is a novel corepressor of HTLV-1 replication and controls viral
989 latency. Blood 121:791-800.
990 56. Decorsiere A, Mueller H, van Breugel PC, Abdul F, Gerossier L, Beran RK,
991 Livingston CM, Niu C, Fletcher SP, Hantz O, Strubin M. 2016. Hepatitis B
992 virus X protein identifies the Smc5/6 complex as a host restriction factor. Nature
993 531:386-9.
994 57. Murphy CM, Xu Y, Li F, Nio K, Reszka-Blanco N, Li X, Wu Y, Yu Y, Xiong
995 Y, Su L. 2016. Hepatitis B Virus X Protein Promotes Degradation of SMC5/6 to
996 Enhance HBV Replication. Cell Rep 16:2846-2854.

997 58. Levrero M, Zucman-Rossi J. 2016. Mechanisms of HBV-induced hepatocellular
998 carcinoma. J Hepatol 64:S84-S101.
999 59. Cha S, Jang KL. 2020. Hepatitis B virus X protein stimulates cell growth by
1000 downregulating p16 levels via PA28gamma-mediated proteasomal degradation.
1001 J Gen Virol 101:963-971.
1002 60. Han J, Kim H, Jeong H, Yoon H, Jang KL. 2021. Proteasomal activator 28
1003 gamma stabilizes hepatitis B virus X protein by competitively inhibiting the
1004 Siah-1-mediated proteasomal degradation. Biochem Biophys Res Commun
1005 578:97-103.
1006 61. Yeom S, Kim SS, Jeong H, Jang KL. 2017. Hepatitis B virus X protein activates
1007 E3 ubiquitin ligase Siah-1 to control virus propagation via a negative feedback
1008 loop. J Gen Virol 98:1774-1784.
1009 62. Boyer LA, Plath K, Zeitlinger J, Brambrink T, Medeiros LA, Lee TI, Levine SS,
1010 Wernig M, Tajonar A, Ray MK, Bell GW, Otte AP, Vidal M, Gifford DK,
1011 Young RA, Jaenisch R. 2006. Polycomb complexes repress developmental
1012 regulators in murine embryonic stem cells. Nature 441:349-53.
1013 63. Brookes E, de Santiago I, Hebenstreit D, Morris KJ, Carroll T, Xie SQ, Stock
1014 JK, Heidemann M, Eick D, Nozaki N, Kimura H, Ragoussis J, Teichmann SA,
1015 Pombo A. 2012. Polycomb associates genome-wide with a specific RNA
1016 polymerase II variant, and regulates metabolic genes in ESCs. Cell Stem Cell
1017 10:157-70.
1018 64. Wakita T, Pietschmann T, Kato T, Date T, Miyamoto M, Zhao Z, Murthy K,
1019 Habermann A, Krausslich HG, Mizokami M, Bartenschlager R, Liang TJ. 2005.
1020 Production of infectious hepatitis C virus in tissue culture from a cloned viral
1021 genome. Nat Med 11:791-6.
1022 65. Kasai H, Kawakami K, Yokoe H, Yoshimura K, Matsuda M, Yasumoto J,
1023 Maekawa S, Yamashita A, Tanaka T, Ikeda M, Kato N, Okamoto T, Matsuura
1024 Y, Sakamoto N, Enomoto N, Takeda S, Fujii H, Tsubuki M, Kusunoki M,
1025 Moriishi K. 2015. Involvement of FKBP6 in hepatitis C virus replication. Sci
1026 Rep 5:16699.
1027 66. Duttweiler HM. 1996. A highly sensitive and non-lethal beta-galactosidase plate
1028 assay for yeast. Trends Genet 12:340-1.

1029 67. Kao SH, Wang WL, Chen CY, Chang YL, Wu YY, Wang YT, Wang SP,
1030 Nesvizhskii AI, Chen YJ, Hong TM, Yang PC. 2015. Analysis of Protein
1031 Stability by the Cycloheximide Chase Assay. Bio Protoc 5.
1032 68. Kikuchi K, Kasai H, Watanabe A, Lai AY, Kondo M. 2008. IL-7 specifies B
1033 cell fate at the common lymphoid progenitor to pre-proB transition stage by
1034 maintaining early B cell factor expression. J Immunol 181:383-92.
1035 69. Sakurai N, Inamochi Y, Inoue T, Hariya N, Kawamura M, Yamada M, Dey A,
1036 Nishiyama A, Kubota T, Ozato K, Goda T, Mochizuki K. 2017. BRD4 regulates
1037 adiponectin gene induction by recruiting the P-TEFb complex to the transcribed
1038 region of the gene. Sci Rep 7:11962.
1039 70. Fujihara Y, Ikawa M. 2014. CRISPR/Cas9-based genome editing in mice by
1040 single plasmid injection. Methods Enzymol 546:319-36.
1041

Fig. 1

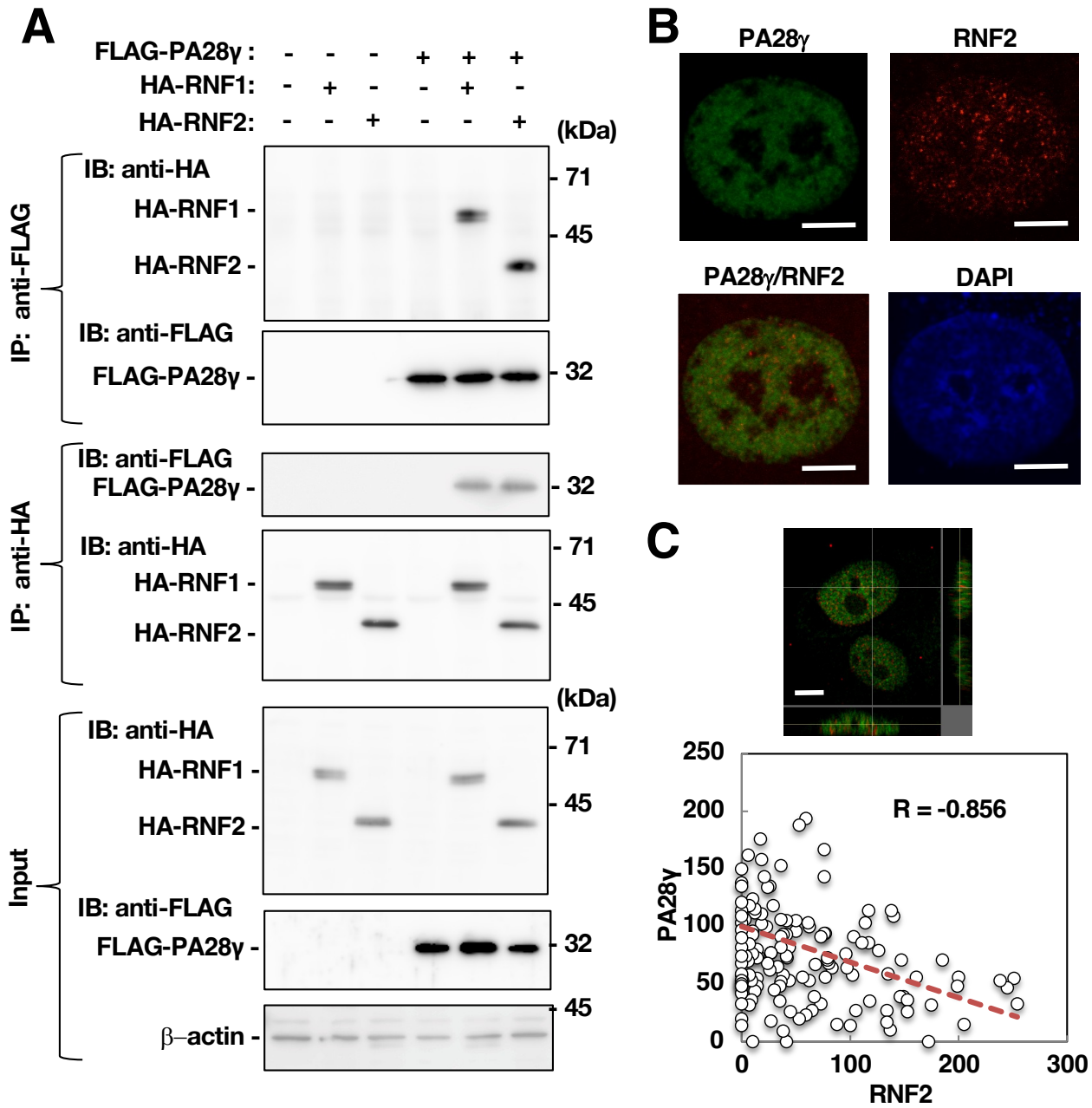
A
FLAG-PA28γ : - - - + + +
HA-RNF1: - + - - + -
HA-RNF2: - - + - - +
(kDa)
IP: anti-FLAG
IB: anti-HA
HA-RNF1 -
HA-RNF2 -
IB: anti-FLAG
FLAG-PA28γ -
71
45
32
IP: anti-HA
IB: anti-FLAG
FLAG-PA28γ -
IB: anti-HA
HA-RNF1 -
HA-RNF2 -
Input
IB: anti-HA
HA-RNF1 -
HA-RNF2 -
IB: anti-FLAG
FLAG-PA28γ -
β–actin -
B
PA28γ
RNF2
PA28γ/RNF2
DAPI
C
R = -0.856
PA28γ
RNF2
250
200
150
100
50
0
0
100
200
300

Fig. 2

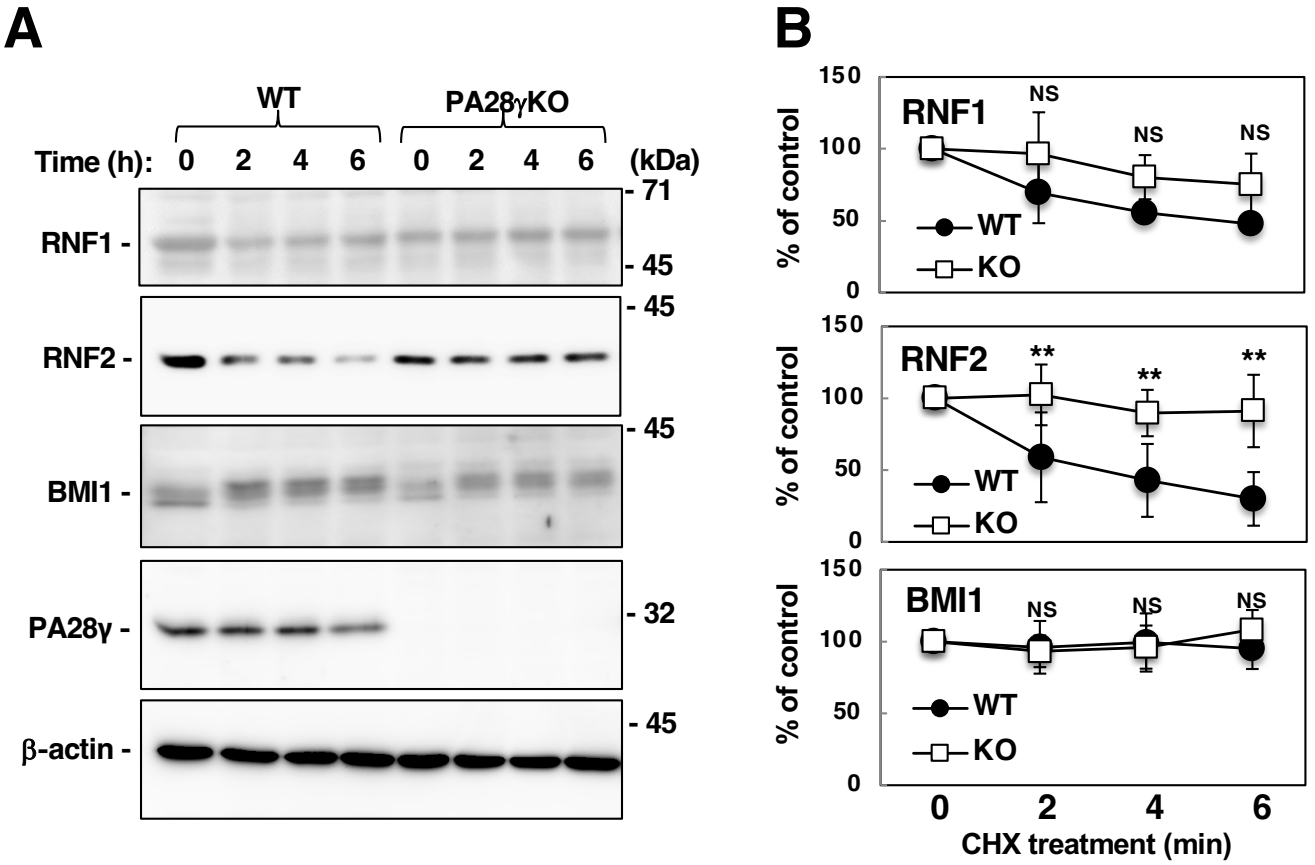
A
WT
PA28γKO
Time (h): 0 2 4 6 0 2 4 6
(kDa)
RNF1 -
- 71
- 45
RNF2 -
- 45
BMI1 -
- 45
PA28γ -
- 32
β-actin -
- 45
B
RNF1
RNF2
BMI1
% of control
150
100
50
0
NS
**
WT
KO
0 2 4 6
CHX treatment (min)

Fig. 3

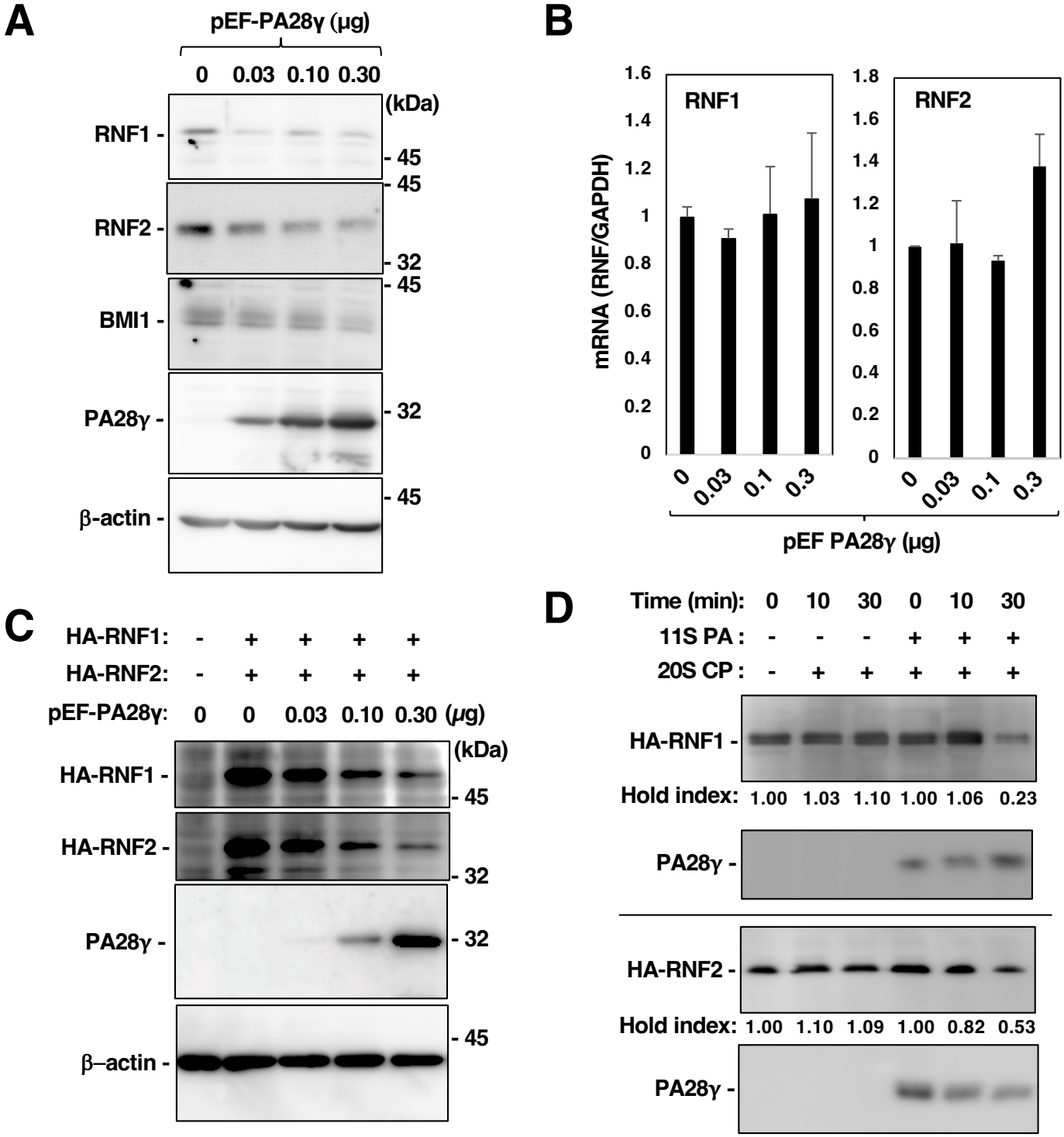
A
pEF-PA28γ (μg)
0 0.03 0.10 0.30
(kDa)
RNF1 -
- 45
RNF2 -
- 45
- 32
BMI1 -
- 45
PA28γ -
- 32
β-actin -
- 45
B
RNF1
RNF2
mRNA (RNF/GAPDH)
0 0.03 0.1 0.3
pEF PA28γ (μg)
C
HA-RNF1: - + + + +
HA-RNF2: - + + + +
pEF-PA28γ: 0 0 0.03 0.10 0.30 (μg)
(kDa)
HA-RNF1 -
- 45
HA-RNF2 -
- 32
PA28γ -
- 32
β–actin -
- 45
D
Time (min): 0 10 30 0 10 30
11S PA : - - - + + +
20S CP : - + + + + +
HA-RNF1 -
Hold index: 1.00 1.03 1.10 1.00 1.06 0.23
PA28γ -
HA-RNF2 -
Hold index: 1.00 1.10 1.09 1.00 0.82 0.53
PA28γ -

Fig. 4

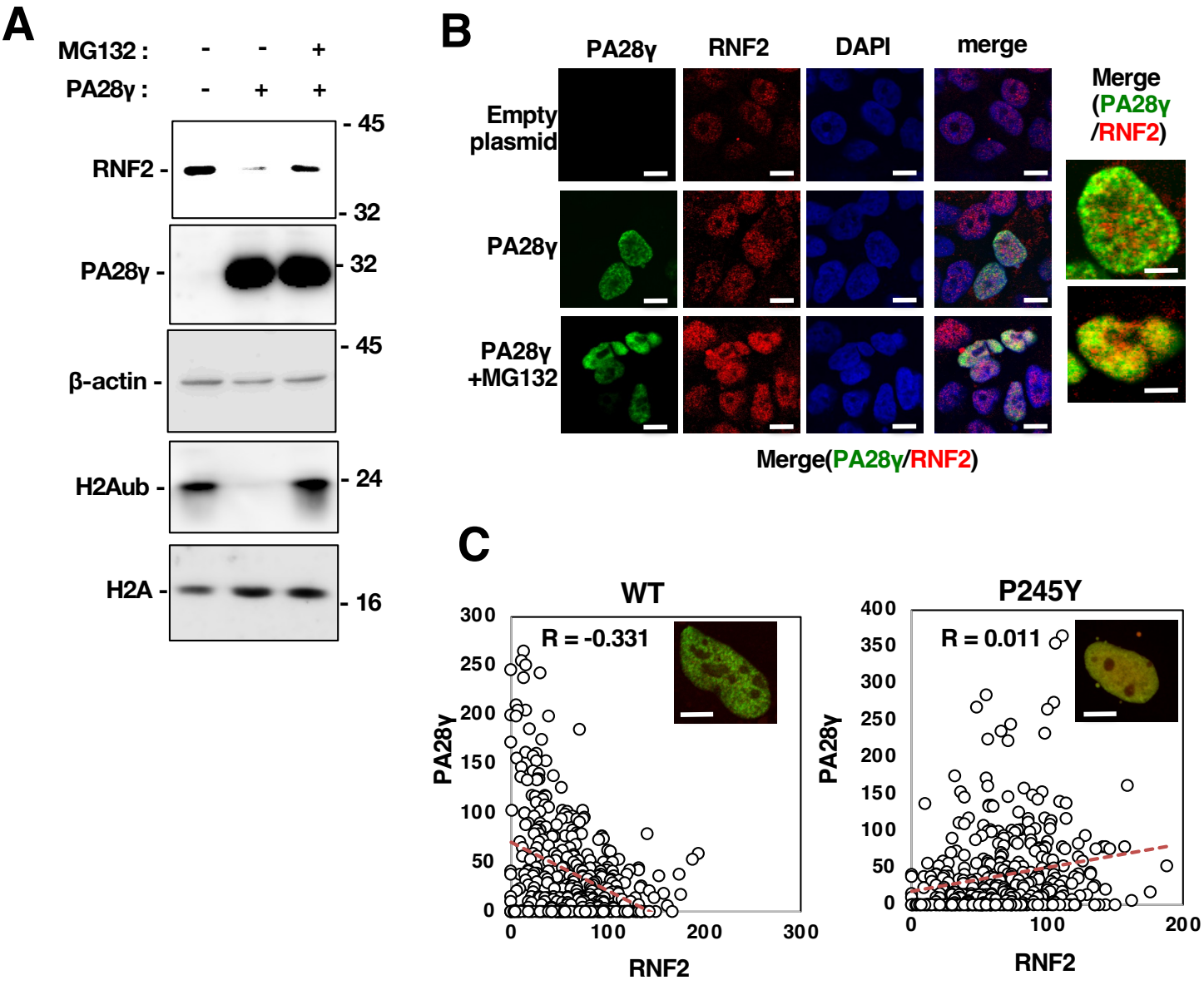
A
MG132 : - - +
PA28γ : - + +
RNF2 -
- 45
- 32
PA28γ -
- 32
β-actin -
- 45
H2Aub -
- 24
H2A -
- 16
B
PA28γ
RNF2
DAPI
merge
Empty plasmid
PA28γ
PA28γ +MG132
Merge (PA28γ /RNF2)
Merge(PA28γ/RNF2)
C
WT
R = -0.331
PA28γ
RNF2
P245Y
R = 0.011
PA28γ
RNF2

Fig. 5

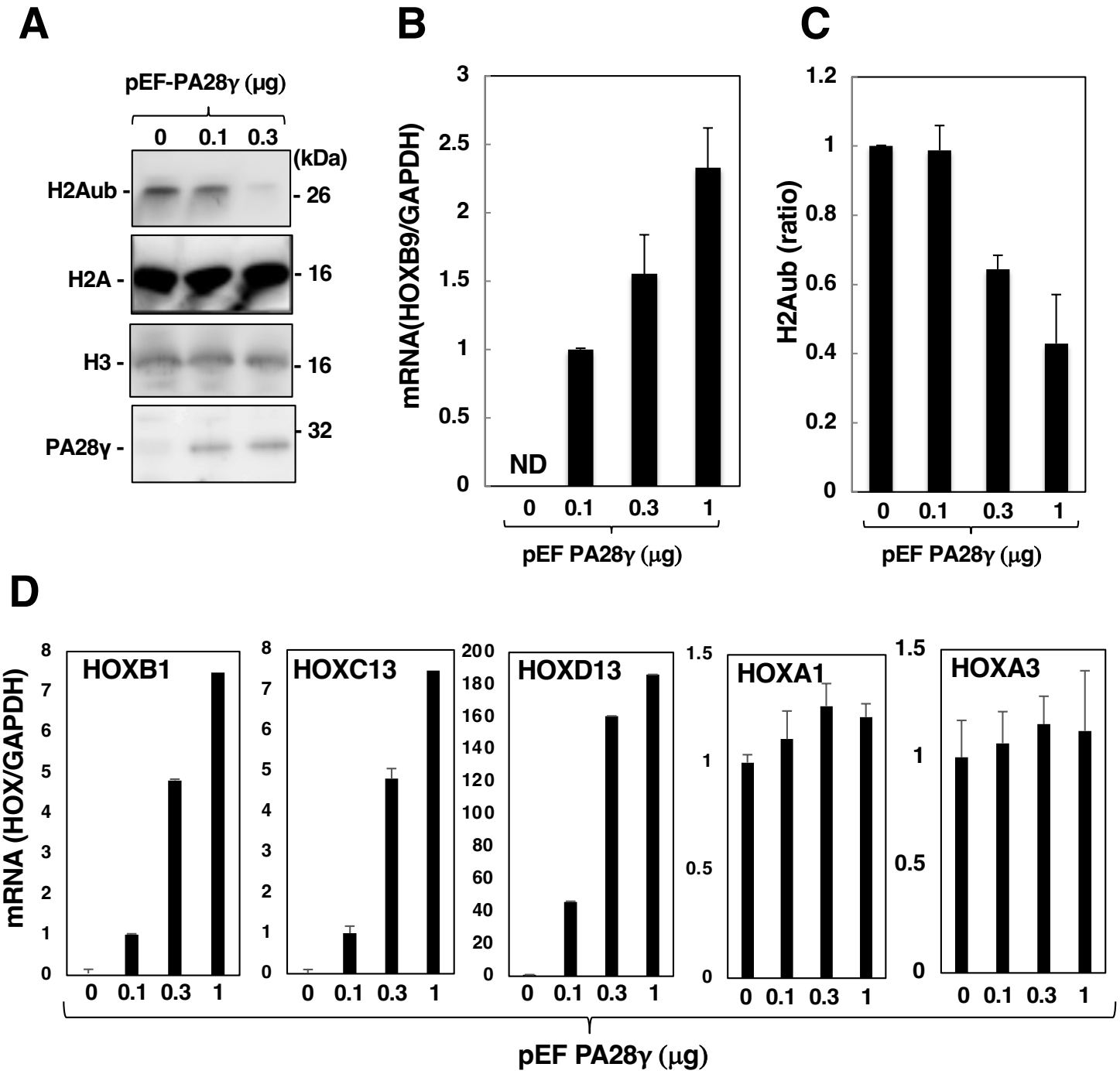
A
pEF-PA28γ (μg)
0 0.1 0.3
(kDa)
H2Aub -
- 26
H2A -
- 16
H3 -
- 16
PA28γ -
- 32
B
mRNA(HOXB9/GAPDH)
ND
0 0.1 0.3 1
pEF PA28γ (μg)
C
H2Aub (ratio)
0 0.1 0.3 1
pEF PA28γ (μg)
D
mRNA (HOX/GAPDH)
HOXB1
HOXC13
HOXD13
HOXA1
HOXA3
0 0.1 0.3 1
pEF PA28γ (μg)

Fig. 6

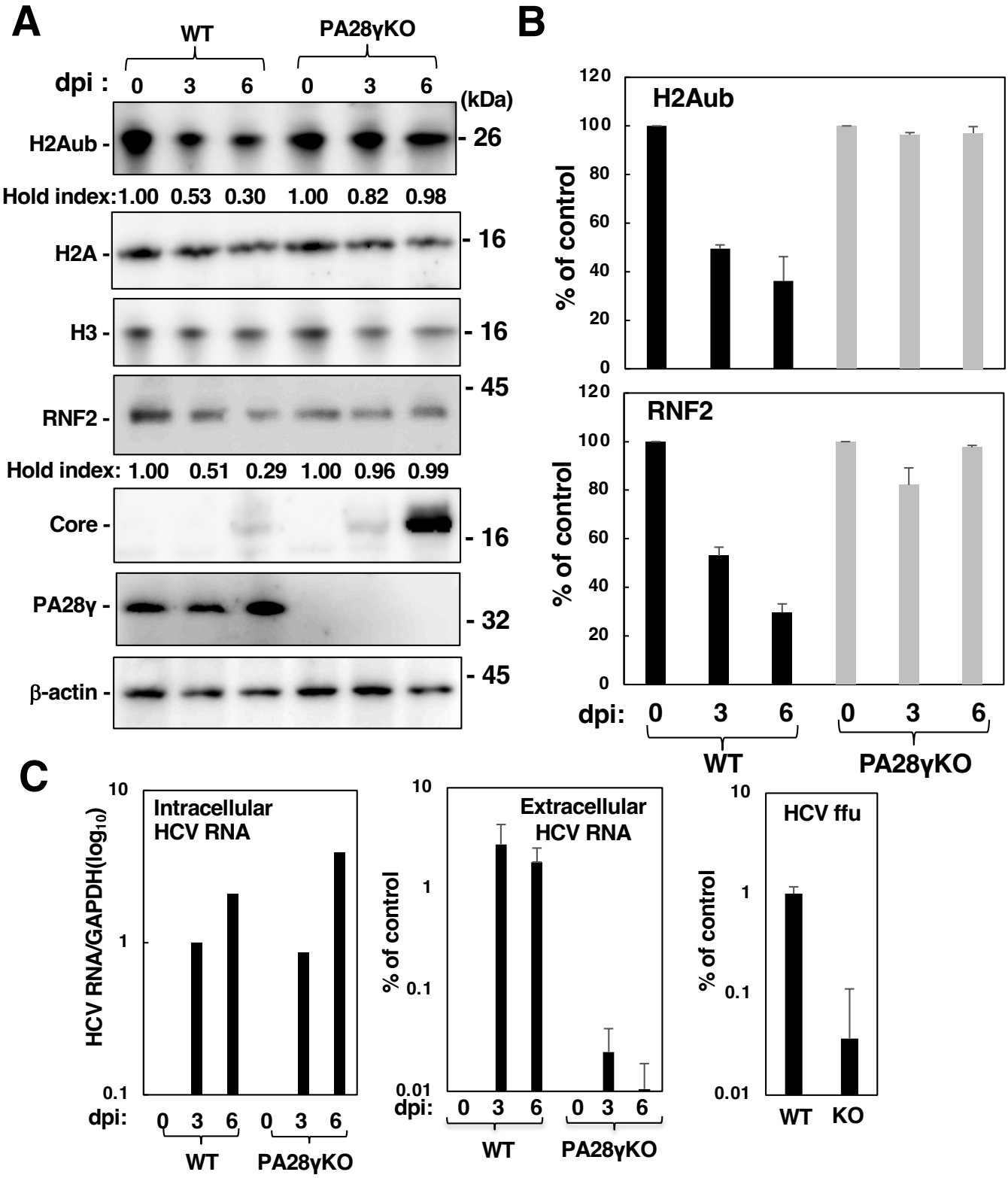
A
WT
PA28γKO
dpi : 0 3 6 0 3 6
(kDa)
H2Aub -
- 26
Hold index: 1.00 0.53 0.30 1.00 0.82 0.98
H2A -
- 16
H3 -
- 16
RNF2 -
- 45
Hold index: 1.00 0.51 0.29 1.00 0.96 0.99
Core -
- 16
PA28γ -
- 32
β-actin -
- 45
B
H2Aub
% of control
RNF2
dpi: 0 3 6 0 3 6
WT
PA28γKO
C
Intracellular HCV RNA
HCV RNA/GAPDH(log10)
dpi: 0 3 6 0 3 6
WT
PA28γKO
Extracellular HCV RNA
% of control
dpi: 0 3 6 0 3 6
WT
PA28γKO
HCV ffu
% of control
WT
KO

Fig. 7

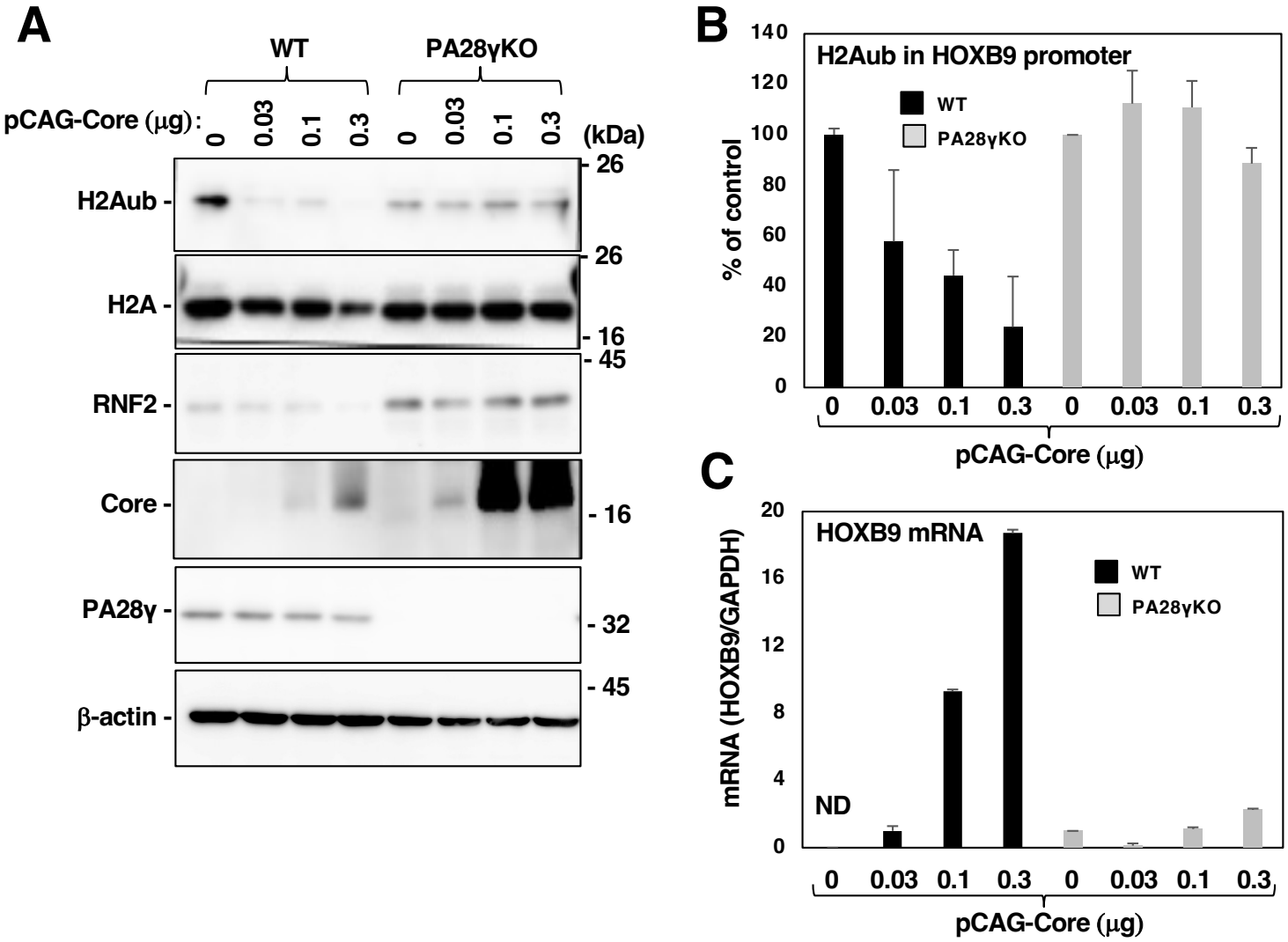
A
WT
PA28γKO
pCAG-Core (μg):
0
0.03
0.1
0.3
0
0.03
0.1
0.3
(kDa)
H2Aub
26
H2A
26
16
RNF2
45
Core
16
PA28γ
32
β-actin
45
B
H2Aub in HOXB9 promoter
WT
PA28γKO
% of control
140
120
100
80
60
40
20
0
0
0.03
0.1
0.3
0
0.03
0.1
0.3
pCAG-Core (μg)
C
HOXB9 mRNA
WT
PA28γKO
mRNA (HOXB9/GAPDH)
20
16
12
8
4
0
ND
0
0.03
0.1
0.3
0
0.03
0.1
0.3
pCAG-Core (μg)

Fig. 8

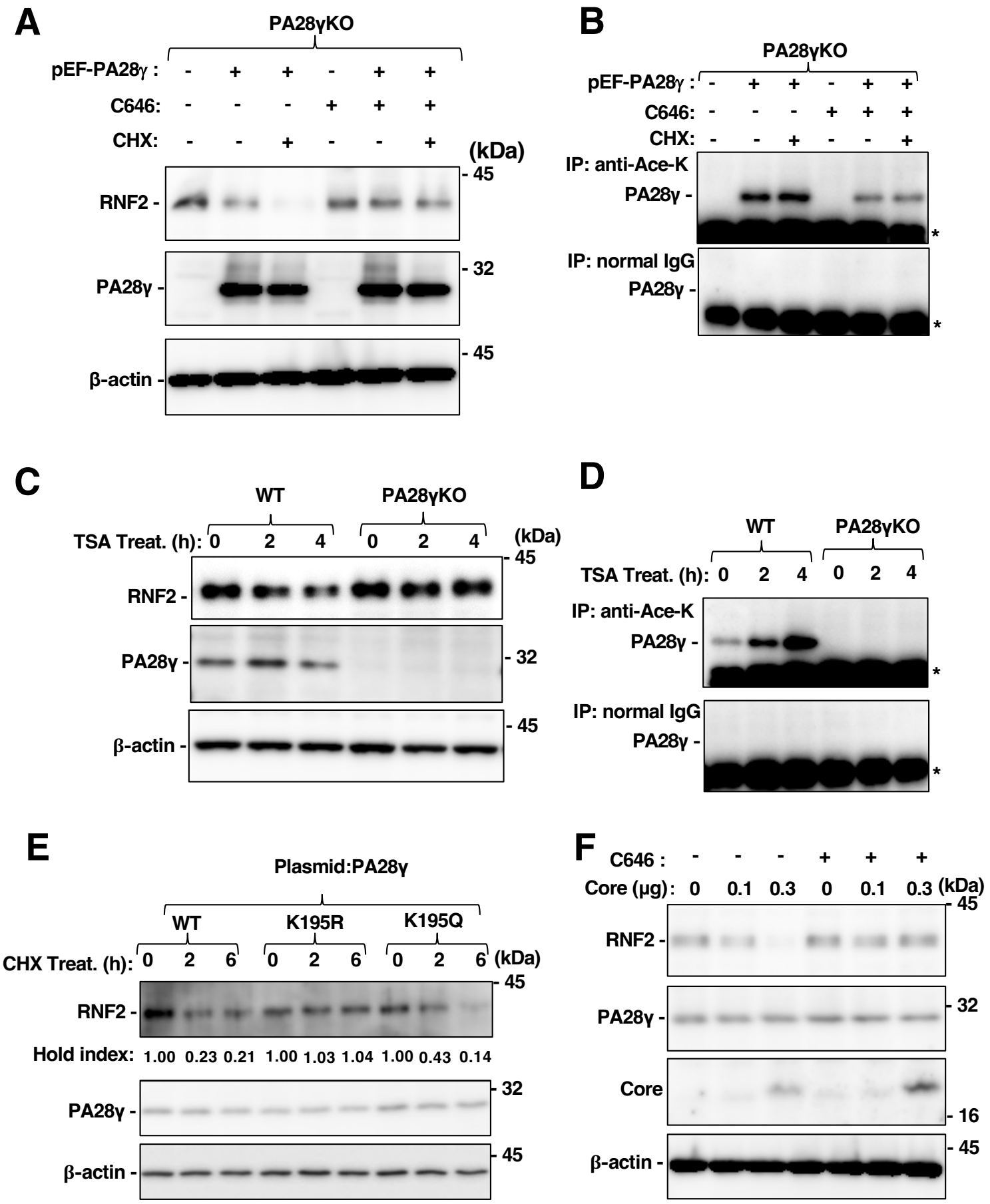
A
PA28γKO
pEF-PA28γ : - + + - + +
C646: - - - + + +
CHX: - - + - - +
(kDa)
RNF2 -
- 45
PA28γ -
- 32
β-actin -
- 45
B
PA28γKO
pEF-PA28γ : - + + - + +
C646: - - - + + +
CHX: - - + - - +
IP: anti-Ace-K
PA28γ -
*
IP: normal IgG
PA28γ -
*
C
WT
PA28γKO
TSA Treat. (h): 0 2 4 0 2 4
(kDa)
RNF2 -
- 45
PA28γ -
- 32
β-actin -
- 45
D
WT
PA28γKO
TSA Treat. (h): 0 2 4 0 2 4
IP: anti-Ace-K
PA28γ -
*
IP: normal IgG
PA28γ -
*
E
Plasmid:PA28γ
WT
K195R
K195Q
CHX Treat. (h): 0 2 6 0 2 6 0 2 6
(kDa)
- 45
RNF2 -
Hold index: 1.00 0.23 0.21 1.00 1.03 1.04 1.00 0.43 0.14
PA28γ -
- 32
β-actin -
- 45
F
C646 : - - - + + +
Core (μg): 0 0.1 0.3 0 0.1 0.3
(kDa)
- 45
RNF2 -
PA28γ -
- 32
Core
- 16
β-actin -
- 45

Fig. 9

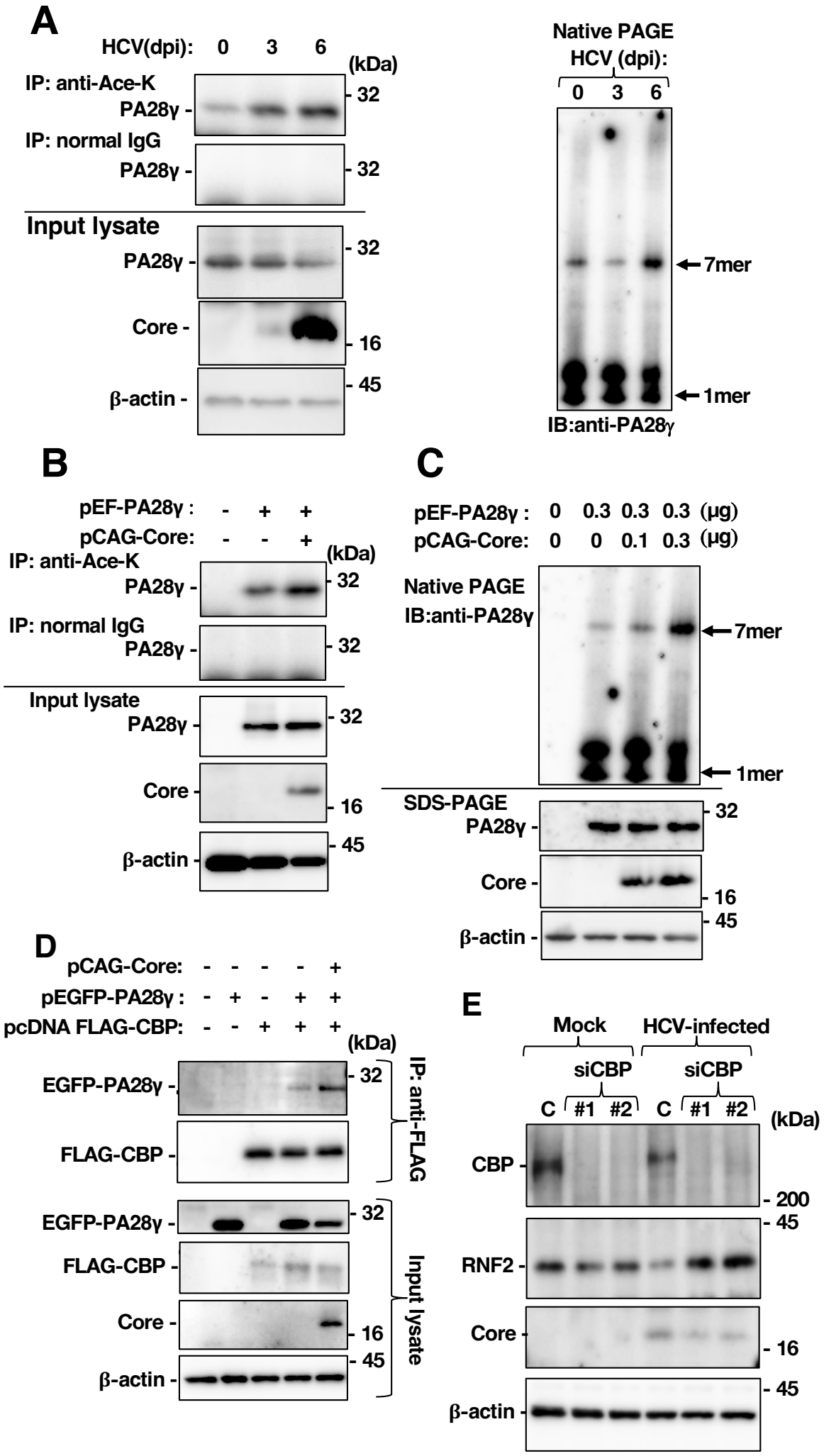
A
HCV(dpi): 0 3 6
(kDa)
IP: anti-Ace-K
PA28γ -
32
IP: normal IgG
PA28γ -
32
Input lysate
PA28γ -
32
Core -
16
β-actin -
45
Native PAGE
HCV (dpi):
0 3 6
7mer
1mer
IB:anti-PA28γ
B
pEF-PA28γ : - + +
pCAG-Core: - - +
(kDa)
IP: anti-Ace-K
PA28γ -
32
IP: normal IgG
PA28γ -
32
Input lysate
PA28γ -
32
Core -
16
β-actin -
45
C
pEF-PA28γ : 0 0.3 0.3 0.3 (μg)
pCAG-Core: 0 0 0.1 0.3 (μg)
Native PAGE
IB:anti-PA28γ
7mer
1mer
SDS-PAGE
PA28γ -
32
Core -
16
β-actin -
45
D
pCAG-Core: - - - - +
pEGFP-PA28γ : - + - + +
pcDNA FLAG-CBP: - - + + +
(kDa)
EGFP-PA28γ -
32
FLAG-CBP -
IP: anti-FLAG
EGFP-PA28γ -
32
FLAG-CBP -
Core -
16
β-actin -
45
Input lysate
E
Mock
HCV-infected
siCBP
siCBP
C #1 #2 C #1 #2
(kDa)
CBP -
200
45
RNF2 -
Core -
16
β-actin -
45

Fig. 10

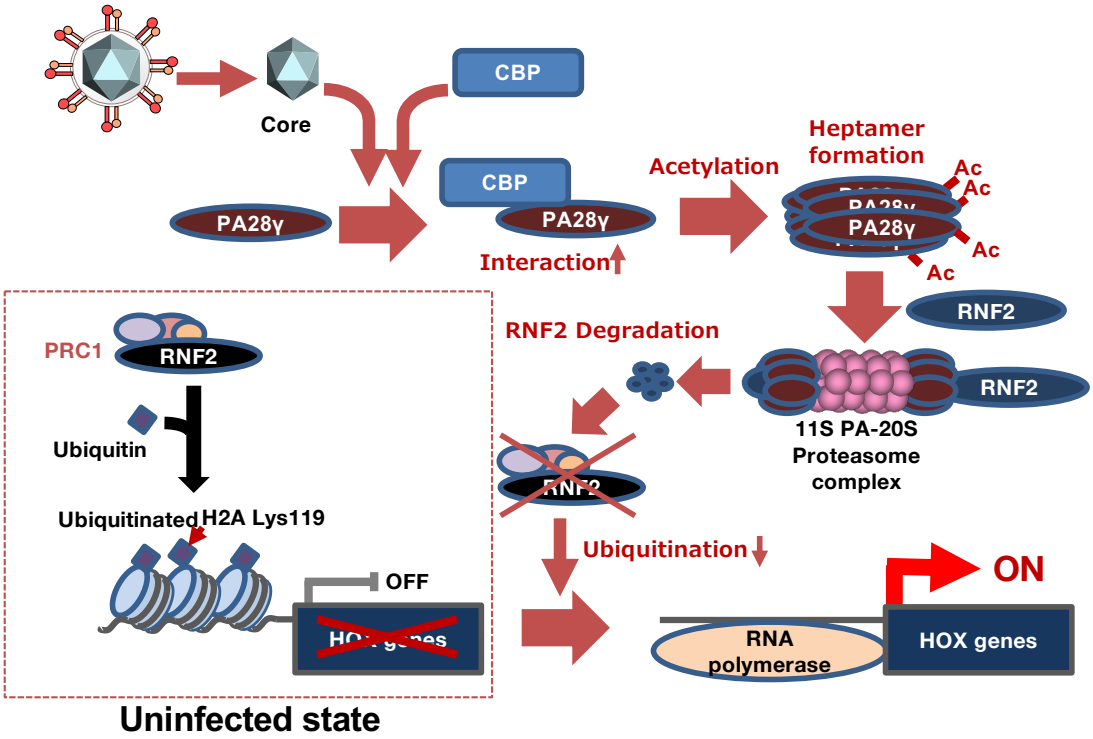
Core
CBP
CBP
PA28γ
PA28γ
Interaction
Acetylation
Heptamer formation
Ac
Ac
PA28γ
Ac
Ac
RNF2
RNF2
11S PA-20S Proteasome complex
RNF2 Degradation
PRC1
RNF2
Ubiquitin
Ubiquitinated H2A Lys119
OFF
Ubiquitination
ON
RNA polymerase
HOX genes
Uninfected state